Chapter 4

STUDIES ON A SERIES OF COPPER BASED ORGANIC-INORGANIC HYBRID COMPOUNDS (OIHCs): A_2CuCl_4 (Achiral)

Abstract

In this chapter we focused on ten OIHCs having the chemical formula A_2CuCl_4, which are investigated for structural phase transition using TG/DTA measurements, DSC studies, single crystal XRD and temperature dependent Raman study, and magnetic measurements using SQUID magnetometer. DSC analyses showed reversible solid-solid phase transition for some OIHCs. The order-disorder phase transition present in the OIHCs correlated to the changes in different degradation pathways. For the confirmation of solid-solid phase transition observed in DSC we have carried out temperature dependent Raman spectroscopy and observed solid-solid phase transition between 260 K - 270 K for compound (4-chloroanilinium)$_2CuCl_4$ (**3**). For the further confirmation of phase transitions in compounds **3**, we have collected single crystal data at different temperature. At 296 K it crystallized in monoclinic space group $P2_1/c$ (inorganic layer, eclipsed configuration) and at 150 K crystallized in orthorhombic space group *Pccn* (inorganic layer, staggered configuration), which proved this solid-solid phase change due to structural change. Single crystal XRD studies for other OIHCs showed that they have forming layered structure of CuCl42- [except (3-chloroanilinium)$_8[CuCl_6]Cl_4$ (**4**) and (2-aminobenzothiazolium)$_2CuCl_4$ (**10**)]. Phase transition observed in compounds **3**, (3-nitro anilinium)$_2CuCl_4$ (**6**), (benzilinium)$_2CuCl_4$ (**7**) and **10** correspond to thermochromic behavior. Temperature dependent EPR spectra and single crystal XRD study revealed thermochromic behavior of compound **10** at 356 K due to structural changes. The dc and ac-magnetic susceptibility measurement using a SQUID magnetometer suggest that these are soft ferromagnets and represent onset of long range magnetic ordering.

4.1 Introduction

As mentioned in earlier chapter, compounds having general formula A_2CuCl_4, belongs to one of the most extensively studied crystalline families of OIHCs [1,2,3], the topic for this chapter. The tetrahalocuprate (II) complexes having different OACs shows varieties of geometry, around the central metal atom and are influenced by non-covalent interactions such as hydrogen bonding [4]. The hydrogen bond driven orientation of organic ammonium molecules force these complexes to undergo interesting structural phase transitions with the change of Cu-X-Cu and X-Cu-X bond angles [5,6,7]. It is found that an angle of Cu-X-Cu, X-Cu-X distance between Cu-Cu, and hydrogen bonding amongst the X and ammonium part of OACs play a crucial role for multifunctional behavior in these classes of compounds. So due to the crucial role of hydrogen bonding in OACs this chapter is restricted to study their effect on $CuCl_4^{2-}$. Is it possible to have perfect square-planar or tetrahedral geometry of tetrahalocuprate (II) stabilized by a hydrogen bonding network of OACs? Because of most of the literature reports CuX_4^{2-} anions with distorted tetrahedral geometries with trans X-Cu-X angles close to 130º. The CuX_4^{2-} ion does not have a regular tetrahedral geometry due to the Jahn-Teller distortion. Thus, the preliminary goal is to study hydrogen bonding in these OIHCs and correlate structure property relationship. The high temperature thermal degradation studies on these compounds are as compared less explored in the literature [8].

Herein, we present the syntheses, thermal degradation pathways, thermochromic behavior, crystal structure and magnetic behavior in OIHCs with general formula A_2CuCl_4. In this work, we have observed evidence of structural phase transition in aromatic layered distorted perovskite type compounds using DSC measurement, Raman spectra, EPR spectra and single crystal XRD.

4.2 Experimental

4.2.1 *Materials and Methods*

All chemicals and solvents used were of analytical grade reagents. Aniline, benzyl amine (s. d. fine); 3-nitro aniline, 4-nitro aniline (spectrochem); 4-fluoro aniline (chemport); 3-chloro aniline, 4-chloro aniline, 4-chloro benzyl amine, 2-

adamantanamidinium chloride, 2-amino benzothiazole and copper (II) chloride (Aldrich); conc. hydrochloric acid (qualigens) and ethyl alcohol (Baroda chemicals) were used as received.

4.2.2 Syntheses of OIHCs: (A_2CuCl_4)

A_2CuCl_4, a type OIHCs were synthesized by a slight modification of the reported procedure by M. G. El-Shaarawy [9]. A general methodology of OIHCs preparation/syntheses is mentioned in scheme-II.

Scheme-II

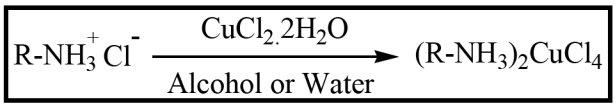

[Where, R = 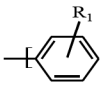 , 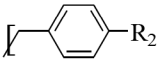 , {R_1 = H (**1**), R_1 = F (*p*-substituted) (**2**), R_1 = Cl (*p*- substituted) (**3**), R_1 = Cl (*m*- substituted) (**4**), R_1 = NO_2 (*p*- substituted) (**5**), R_1 = NO_2 (*m*- substituted) (**6**), R_2 = H (**7**) and R_2 = Cl (**8**)},  (**9**), and [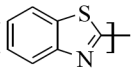 (**10**)]

In actual process the OIHCs [(anilinium)$_2CuCl_4$ (**1**)] was prepared in nitrogen environment by dissolving the appropriate amount (2:1 ratio) 350.0 mg (2.700 mmol) of aniline hydrochloride and 230.0 mg (1.350 mmol) of $CuCl_2.2H_2O$ in acidified distilled water. Subsequently the solution was heated at 373 K approximately 3 - 4 hours. Evaporation of water was carried out using vacuum pump. The precipitates were rinsed with ether and recrystallized in ethanol by slow evaporation technique. After 1 - 2 weeks good quality crystals suitable for single crystal XRD were obtained.

Yield: 40 - 60 %

4.3 Results and Discussions

4.3.1 General Discussion

A_2CuCl_4 compounds crystallize in different crystal systems ranging from tetragonal to triclinic ones [10,11]. During this $CuCl_4^{2-}$ anion changes to all possible geometries tetrahedral, octahedral and isolated square-planar structures, mainly controlled by the ligand. Compounds **1, 2**, **3**, and **10**, known in the literature, and are crystallized in the monoclinic space group $P2_1/c$ [12], while at lower temperature compound **3** adopts space group *Pccn* and resembles very much with compounds **7**, **8**.

Most of these compounds form $CuCl_4^{2-}$ perovskite sheets with Cu-Cl-Cu angles varying from 164.4(1)º for compound **1** [13], 163.4(1)º for compound **2**, 167.7(1)º for compound **3**, 176.3(3)º for compound **8** and 180.0(1)º for $(NH_4)_2CuCl_4$ [14]. The observed Cu-Cl distances and Cu-Cl-Cu angles are shown in Table 4.1. The origin of the change in Cu-Cl-Cu angle lies in the interaction between organic and inorganic components. This interaction is due to van der Waals force, the hydrogen bonds between the ammonium group of the organic moiety and the chlorine atom in the inorganic layer. This results in observed puckering of the layer. The change in the bonding scheme has been triggered by the reorientational motion and conformational changes of the organic groups. This attributes weakening of the N-H···Cl bonding with increasing temperature which is believed to be a decrease in the tilting of the $CuCl_6^{4-}$ octahedra. It could also be associated with a change in the amount of the tetragonal distortion of the $CuCl_6^{4-}$ octahedra. This is one of the reasons for the change observed in the color of the compound **3**. This compound undergoes two thermochromic transitions orange phase to (T = 294 K) yellow phase to (T = 214 K) green phase [15]. DSC study on compound **6** shows one phase transition as reported in the literature, but no thermochromic behavior [16].

Table 4.1 Crystal parameters for layered OIHCs

Compounds	Crystal System	Cu-Cl Distance [Å]	M-M Distance [Å] Inter	Intra	M-X-M Angle [°]
$(NH_4)_2CuCl_4$ [14]	Orthorhombic *Cmca*	2.793(5) 2.332(4) 2.0300(5)			180.0(2)
1 [13]	Monoclinic *P2₁/c*	2.9178(5) 2.3007(5) 2.2804(6)	15.05(1)		164.4(1)
2	Monoclinic *P2₁/c*	2.876(2) 2.284(2)	16.511(1)	5.118(1)	163.4(1)
3	Monoclinic *P2₁/c*	2.906(2) 2.307(2)	16.434(1)	5.181(2)	167.7(1)
3'	Orthorhombic *Pccn*	2.885(1) 2.275(1)	16.429(2)	5.139(1)	164.5(1)
4 [11]	Triclinic *P-1*	2.6061(18) 2.6086(20) 2.2773(11)	14.273(7)	8.5488(16)	
5 [17]	Orthorhombic *Pbca*	3.075(2) 2.303(2)	16.230(1)		
8	Monoclinic *Cc*	2.682(5) 2.628(5) 2.623(5) 2.609(5) 2.271(3) 2.270(3)	16.961(4)	5.288(2) 5.244(2)	176.3(3) 174.5(2)
10	Monoclinic *P2₁/c*	2.2724(6) 2.2663(5)	8.5397(3)	7.0562(3)	
10'	Monoclinic *P2₁/c*	2.2723(5) 2.2692(4)	8.4894(3)	6.9522(4)	
$(C_6H_5CH_2CH_2NH_3)_2$ $CuCl_4$ [18]	Orthorhombic *Pbca*	2.8531(9) 2.2879(9) 2.3036(8)		5.188(2)	169.15(3)

4.3.2 FT-IR Spectra

Analytical data for the OIHCs are given below.

1: FT-IR (KBr) 2997 (vs), 2899 (m), 2578 (w), 1767 (w), 1759 (m), 1614 (w), 1603 (m), 1555 (s), 1509 (m), 1493 (ssh), 1340 (w), 1321 (m), 1285 (m), 1242 (m), 1201 (m), 1102 (s), 1043 (m), 1025 (m), 989 (w), 806 (w), 738 (ssh), 681 (vssh), 620 (w), 526 (m) and 475 (s) cm^{-1}.

2: FT-IR (KBr) 3434 (s), 3024 (vs), 2577 (s), 2365 (w), 1869 (w), 1623 (s), 1562 (s), 1498 (vs), 1291 (w) 1245 (vssh), 1201 (m), 1157 (m), 1101 (s), 1049 (m), 1016 (m), 819 (ssh), 737 (m), 636 (w), 502 (s), 459 (m), and 432 (m) cm^{-1}.

3: FT-IR (KBr) 3448 (w), 3047 (vs), 2573 (m), 1885 (w), 1611 (w), 1553 (m), 1488 (s), 1312 (w), 1281 (w), 1195 (w), 1095 (s), 1070 (m), 1016 (w), 810 (s), 640 (w) and 488 (m) cm^{-1}.

4: FT-IR (KBr) 3023 (vs), 2905 (s), 2583 (s), 1777 (w), 1597 (m), 1562 (s), 1501 (s), 1475 (s), 1445 (m), 1283 (m), 1082 (m), 1059 (w), 971 (w), 887 (m), 864 (s), 771 (ssh), 669 (vssh), 526 (m), 436 (s) and 411 (s) cm^{-1}.

5: FT-IR (KBr) 3305 (w), 3011 (vs), 2573 (s), 2550 (s), 2299 (m), 2132 (w), 1918 (m), 1785 (m), 1601 (s), 1573 (s), 1537 (s), 1519 (vssh), 1490 (vs), 1429 (s), 1364 (vs), 1348 (s), 1321 (s), 1283 (m), 1181 (w), 1113 (w), 1188 (w), 1167 (m), 1018 (m), 969 (m), 953 (m), 864 (s), 843 (s), 794 (m), 737 (ssh), 669 (s), 633 (m), 533 (m) and 466 (s) cm^{-1}.

6: FT-IR (KBr) 3437 (w), 3031 (vs), 2582 (s), 1780 (w), 1612 (m), 1541 (vs), 1500 (s), 1352 (vssh), 1208 (w), 1104 (m), 910 (w), 805 (m), 732 (ssh), 663 (m) and 489 (w) cm^{-1}.

7: FT-IR (KBr) 3154 (vs), 2885 (s), 2574 (m), 2350 (w), 2301 (w), 1958 (w), 1774 (m), 1566 (s), 1488 (s), 1456 (m), 1389 (m), 1313 (w), 1217 (s), 1098 (s), 1050 (m), 1031 (w), 968 (w), 924 (w), 864 (w), 787 (w), 754 (ssh), 701 (ssh), 669 (w), 573 (m) and 486 (m) cm^{-1}.

8: FT-IR (KBr) 3153 (vs), 2884 (w), 2566 (w), 2350 (m), 2300 (w), 1913 (w), 1759 (m), 1601 (m), 1566 (s), 1490 (vssh), 1457 (s), 1387 (s), 1327 (w), 1246 (s), 1214 (s), 1097 (ssh), 1063 (m), 1021 (m), 969 (m), 862 (m), 837 (ssh), 791 (m), 750 (m), 719 (w), 702 (s), 679 (s), 641 (s), 572 (w), 530 (s) and 418 (m) cm^{-1}.

9: FT-IR (KBr) 3048 (s), 2905 (vs), 2860 (vs), 2602 (s), 1593 (s), 1571 (s), 1495 (vs), 1468 (s), 1397 (s), 1191 (m), 1089 (s), 1052 (m), 999 (s), 933 (w), 803 (w), 785 (w), 674 (w), 522 (s) and 435 (s) cm^{-1}.

10: FT-IR (KBr) 3273 (vs), 3103 (vs), 2952 (s), 1951 (w), 1799 (w), 1688 (w), 1652 (vs), 1644 (vs), 1604 (s), 1578 (vs), 1467 (ssh), 1403 (w), 1370 (s), 1304 (w), 1256 (s), 1217 (m), 1096 (w), 1014 (m), 942 (m), 884 (m), 860 (w), 762 (vssh), 710 (s), 698 (s), 646 (s), 598 (s), 558 (s), 518 (m), 498 (s), 482 (s) and 428 (s) cm^{-1}.

FT-IR represents asymmetric stretching modes of N-H ($-NH_3^+$ group) shifted at 3154 - 2997 cm^{-1} and 2602 - 2566 cm^{-1} for OIHCs indicates the braking of continuous series of hydrogen bonds. The other N-H ($-NH_3^+$ group) deformation modes and rocking modes were observed at 1652 - 1611cm^{-1} and 1566 - 1488 cm^{-1} respectively. The bands observed at 1352 - 1245 cm^{-1}/1217 - 1021 cm^{-1} were due to the aromatic/aliphatic C-N stretching. Other modes which provide vital information about the C-H aromatic ring out of plane deformation signifies two and three hydrogen adjacent position at 843 - 810 cm^{-1} and 805 - 771 cm^{-1} respectively. The bands observed at 738 cm^{-1} and 681 cm^{-1} for compound **1** are due to the C-H out-of-plane deformation for four adjacent hydrogen atoms. The bands at 754 cm^{-1} and 701 cm^{-1} for compound **7** are due to C-H out-of-plane deformation for four adjacent hydrogen atoms. In case of compound **10** vibrational band observed at 762 cm^{-1} indicates the C-H out-of-plane deformation for four adjacent hydrogen atoms. The IR band is also observed at 2885 cm^{-1} for compounds **7** and **8** due to aliphatic C-H stretching. The FT-IR spectra of some OIHCs are shown in Figure 4.1.

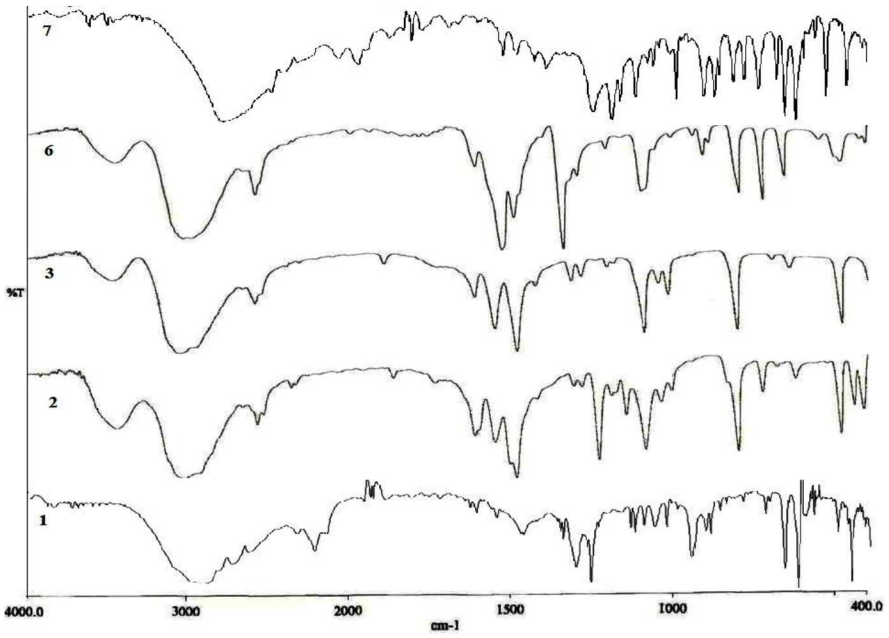

Figure 4.1 Representative FT-IR spectra of compounds **1**, **2**, **3**, **6** and **7**.

4.3.3 Elemental Analyses

The elemental analyses were consistent with the formulae A_2CuCl_4. *Anal.* Ref. sulfanilamide: Found (calc.) %; C, 41.85 (41.81); H, 4.68 (4.65); N, 15.26 (16.25). $(C_6H_5NH_3)_2CuCl_4$ (**1**)**:** Found (calc.) %; C, 36.48 (36.61); H, 3.64 (4.06); N, 6.45 (7.11). $(4\text{-}F\text{-}C_6H_4NH_3)_2CuCl_4$ (**2**)**:** Found (calc.) %; C, 34.15 (33.55); H, 3.02 (3.26); N, 6.32 (6.52). $(4\text{-}Cl\text{-}C_6H_4NH_3)_2CuCl_4$ (**3**)**:** Found (calc.) %; C, 31.50 (31.16); H, 2.91 (3.03); N, 6.00 (6.05). $(4\text{-}NO_2\text{-}C_6H_4NH_3)_2CuCl_4$ (**5**)**:** Found (calc.) %; C, 29.96 (30.32); H, 2.86 (2.94); N, 11.54 (11.77). $(4\text{-}Cl\text{-}C_6H_4CH_2NH_3)_2CuCl_4$ (**8**)**:** Found (calc.) %; C, 34.17 (34.27); H, 3.80 (3.67); N, 5.60 (5.71). $(2\text{-}NH_2\text{-}C_6H_4CSNH)_2CuCl_4$ (**10**)**:** Found (calc.) %; C, 33.41 (33.11); H, 3.00 (2.76); N, 10.91 (11.03).

4.3.4 Thermal Analyses

4.3.4.1 Thermogravimetry/Differential Thermal Analysis (TG/DTA)

TG/DTA analyses were performed on the powdered compounds of layered OIHCs. Figure 4.2 show the thermal analyses of some OIHCs. Compounds **1**, **3**, **5**, **6** and **8** follow a similar degradation pathway as compared to compounds **2**, **4** and **9**, while **7** has the different degradation pathway as tabulated below.

$(C_6H_5NH_3)_2CuCl_4$	$(4\text{-}F\text{-}C_6H_4NH_3)_2CuCl_4$
Temp. 444.1 K ↓ $C_6H_5NH_2HCl + C_6H_5NH_2$	Temp. 491.8 K ↓ $2(4\text{-}F\text{-}C_6H_4NH_2HCl)$
Loss − 56.57 % (theory)	Loss = 68.70 % (theory)
Loss = 58.10 % (found)	Loss = 67.20 % (found)
$(H)CuCl_3$	$CuCl_2$
Temp. 776.4 K ↓ $HCl + Cl_2$	Temp. 790.7 K ↓ Cl_2
Loss = 27.29 % (theory)	Loss = 16.52 % (theory)
Loss = 21.32 % (found)	Loss = 19.05 % (found)
Cu	Cu
16.14 % (theory)	14.79 % (theory)
20.58 % (found)	13.76 % (found)

$(4\text{-Cl-}C_6H_4NH_3)_2CuCl_4$

Temp. 485.1 K ↓ $4\text{-Cl-}C_6H_4NH_2HCl + 4\text{-Cl-}C_6H_4NH_2$
Loss = 63.04 % (theory)
Loss = 65.04 % (found)

$(H)CuCl_3$

Temp. 852.2 K ↓ $HCl + Cl_2$
Loss = 23.23 % (theory)
Loss = 17.08 % (found)

Cu
13.74 % (theory)
17.87 % (found)

$[(3\text{-Cl-}C_6H_4NH_3)_8CuCl_6]Cl_4$

Temp. 454.5 K ↓ $8(3\text{-Cl-}C_6H_4NH_2)$
Loss = 70.54 % (theory)
Loss = 69.80 % (found)

$(H)_8CuCl_{10}$

Temp. 816.0 K ↓ $8HCl$
Loss = 20.17 % (theory)
Loss = 20.20 % (found)

$CuCl_2$
9.30 % (theory)
9.92 % (found)

$(4\text{-}NO_2\text{-}C_6H_4NH_3)_2CuCl_4$

Temp. 453.0 K ↓ $4\text{-}NO_2\text{-}C_6H_4NH_2HCl$ + $4\text{-}NO_2\text{-}C_6H_4NH_2$
Loss = 64.90 % (theory)
Loss = 71.77 % (found)

$(H)CuCl_3$

Temp. 813.5 K ↓ $HCl + Cl_2$
Loss = 22.59 % (theory)
Loss = 21.20 % (found)

Cu
13.36 % (theory)
7.02 % (found)

$(3\text{-}NO_2\text{-}C_6H_4NH_3)_2CuCl_4$

Temp. 474.3 K ↓ $3\text{-}NO_2\text{-}C_6H_4NH_2HCl$ + $3\text{-}NO_2\text{-}C_6H_4NH_2$
Loss = 64.90 % (theory)
Loss = 65.21 % (found)

$(H)CuCl_3$

Temp. 573.0 K to 923.0 K ↓ $HCl + Cl_2$
Loss = 22.59 % (theory)
Loss = 16.33 % (found)

Cu
13.36 % (theory)
18.42 % (found)

$(C_6H_5CH_2NH_3)_2CuCl_4$

Temp. 544.0 K ↓ $2HCl + Cl_2$
Loss = 34.17 % (theory)
Loss = 32.36 % (found)

Temp. 568.8 K ↓ $2C_6H_5CH_2NH_2$
Loss = 50.41 % (theory)
Loss = 53.45 % (found)

Cu
15.09 % (theory)
14.49 % (found)

$(4\text{-Cl-}C_6H_4CH_2NH_3)_2CuCl_4$

Temp. 518.7 K ↓ $4\text{-Cl-}C_6H_4CH_2NH_2HCl$ + $4\text{-Cl-}C_6H_4CH_2NH_2$
Loss = 65.36 % (theory)
Loss = 68.27 % (found)

$(H)CuCl_3$

Temp. 808.4 K ↓ $HCl + Cl_2$
Loss = 21.89 % (theory)
Loss = 19.91 % (found)

Cu
12.95 % (theory)
11.82 % (found)

$(2\text{-Adamantyl-}NH_3)_2CuCl_4$

Temp. 560.3 K ↓ $2(2\text{-Adamantyl-}NH_2)$, Loss = 59.32 % (theory), Loss = 45.90 % (found)

$(H)_2CuCl_4$

Temp. 604.8 K ↓ 2HCl, Loss = 13.92 % (theory), Loss = 24.61 % (found)

$CuCl_2$

26.38 % (theory)

29.50 % (found)

Aniline can act as reducing agent a part of $CuCl_2$ converted into CuCl on heating [8]. In case of compound **1**, DTA shows endothermic peak at 444.1 K because of thermal decomposition. At this temperature, it loses one mole of anilinium chloride along with aniline. Calculation of first weight loss was observed near to the evaporation of anilinium chloride and aniline. After the weight loss of organic ammonium chloride along with amine $(H)CuCl_3$ is left. $[CuCl_3]^-$ species remain in dimeric form if the cations are small which is observed in literature [19]. At HT, 776.4 K, it again loss chlorine molecule in reducing atmosphere of hydrochloric acid to convert Cu. Calculated second weight loss comes very close to the evaporation of HCl and Cl_2 molecule per formula unit but these are not completely evaporated. This decomposition path of compound **1** is very similar to compounds **3**, **5**, **6** and **8**. In case of compound **2**, where initially two moles of 4-fluoro anilinium chloride were lost and then one mole of Cl_2. Compounds **4** and **9** loose organic amine first and then HCl leaving behind $CuCl_2$. The compound **10** shows weight loss at temperature as low as 357 K with bulk decomposition seen around 539 K and 773 K. The major weight loss starts around 473 K, as shown in Figure 4.2 (f). The total weight loss during decomposition corresponds to 57.10 %. This is in good agreement with the complete weight loss of organic component (2-aminobenzothiozole) and stable inorganic component of the compound $(H)_2CuCl_4$ remained at the bottom. On the other hand in case of compound **7** the thermal decomposition path is totally different, here two moles of hydrochloride are lost along with the chlorine molecule in initial heating, instead of benzilinium chloride and benzyl amine and then loses two molecules of

benzyl amine leaving behind Cu above 573 K. The calculation of weight loss comes very close to the evaporation of observed weight loss for all OIHCs. The DTA of compounds **7** and **9** shows exothermic peaks at 544 K and 560 K. Normally exothermic transitions are observed due to crystallization or desolvation/dehydration. In case of compound **7** the exothermic mass loss accounts for Cl_2, a process of dechlorination? Thus, thermal analyses show different thermo chemical reactions operating these compounds which are important for cleavage of bond or rearrangement of ligand.

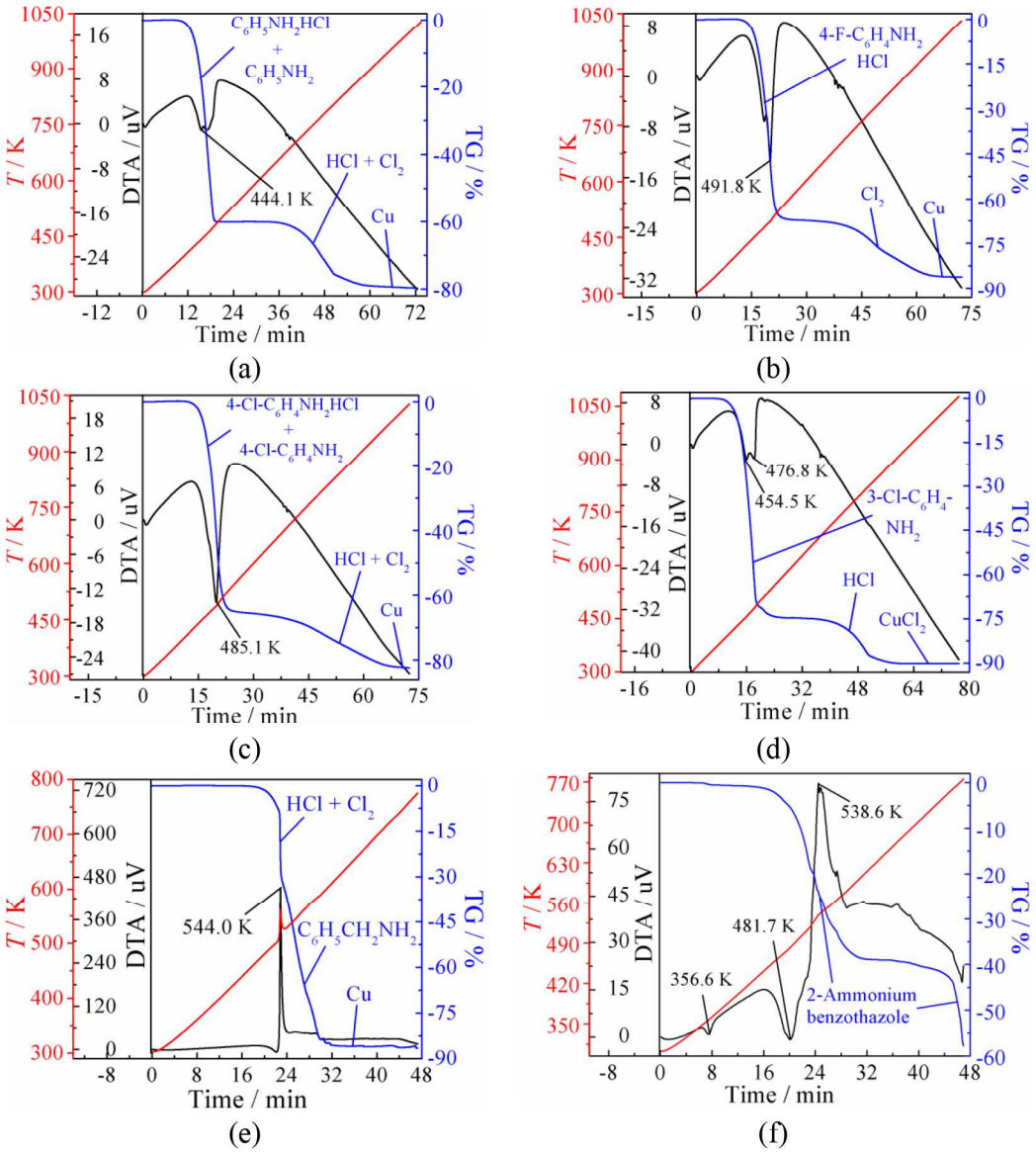

Figure 4.2 Thermo gravimetric curve for compounds **1** (a); **2** (b); **3** (c); **4** (d); **7** (e) and **10** (f).

4.3.4.2 Differential Scanning Calorimetry (DSC)

To confirm our different degradation pathway and exothermic behavior of DTA we carried out DSC on all OACs and their complexes from 153 K to their degradation temperature. DSC studies on OACSs shows absence of solid-solid phase transition after the addition of any substituent on the aromatic ring (except 3-nitro anilinium chloride) in OACSs. But after the syntheses of OIHCs we observed compounds **3**, **4**, **7**, **9** and **10** shows endothermic peak at 275.83 K (-1.72 J g^{-1}), 406.39 K (-1.06 J g^{-1}), 403.95 K (-1.98 J g^{-1}), 470.85 K (-34.75 J g^{-1}) and 356.05 K (-19.31 J g^{-1}) respectively while heating and exothermic peak at 269.48 K (1.42 J g^{-1}), 389.10 K (2.60 J g^{-1}), 390.07 K (0.93 J g^{-1}), 451.03 K (33.14 J g^{-1}) and 305.84 K (1.54 J g^{-1}) respectively while cooling. These peaks are characteristics for solid-solid phase transition (see Figure 4.3). The details of phase changes are given in Table 4.2. These transitions are reversible in nature and can be repeated up to many cycles without any change in peak position. While DSC studies on compounds **1**, **2**, **5** and **8** does not show any signature of solid-solid phase transition. In literature for compounds **1** and **6** phase transitions are observed at 373 K and 400 K respectively [8,16]. But TG measurement for compound **1** shows small mass loss at that region which may be due to the low boiling solvent used for the syntheses by the authors. Furthermore, we measured DSC but not observed any change around this region for compound **1** and observed one solid-solid phase change at 410.5 K (similar temperature with previous report for compound **6**).

Table 4.2 DSC chart of OIHCs

Compounds	Phase Transition			
	Heating		Cooling	
	Temperature [K]	Enthalpy [J g^{-1}]	Temperature [K]	Enthalpy [J g^{-1}]
1	No transition observed			
2	No transition observed			
3	275.83	-1.72	269.48	1.42
4	404.39	-1.06	389.10	2.60
5	No transition observed			
6	410.50	-	-	-
7	403.95	-1.98	390.07	0.93
8	No transition observed			
9	470.85	-34.75	451.03	33.14
10	356.05	-19.31	305.84	1.54

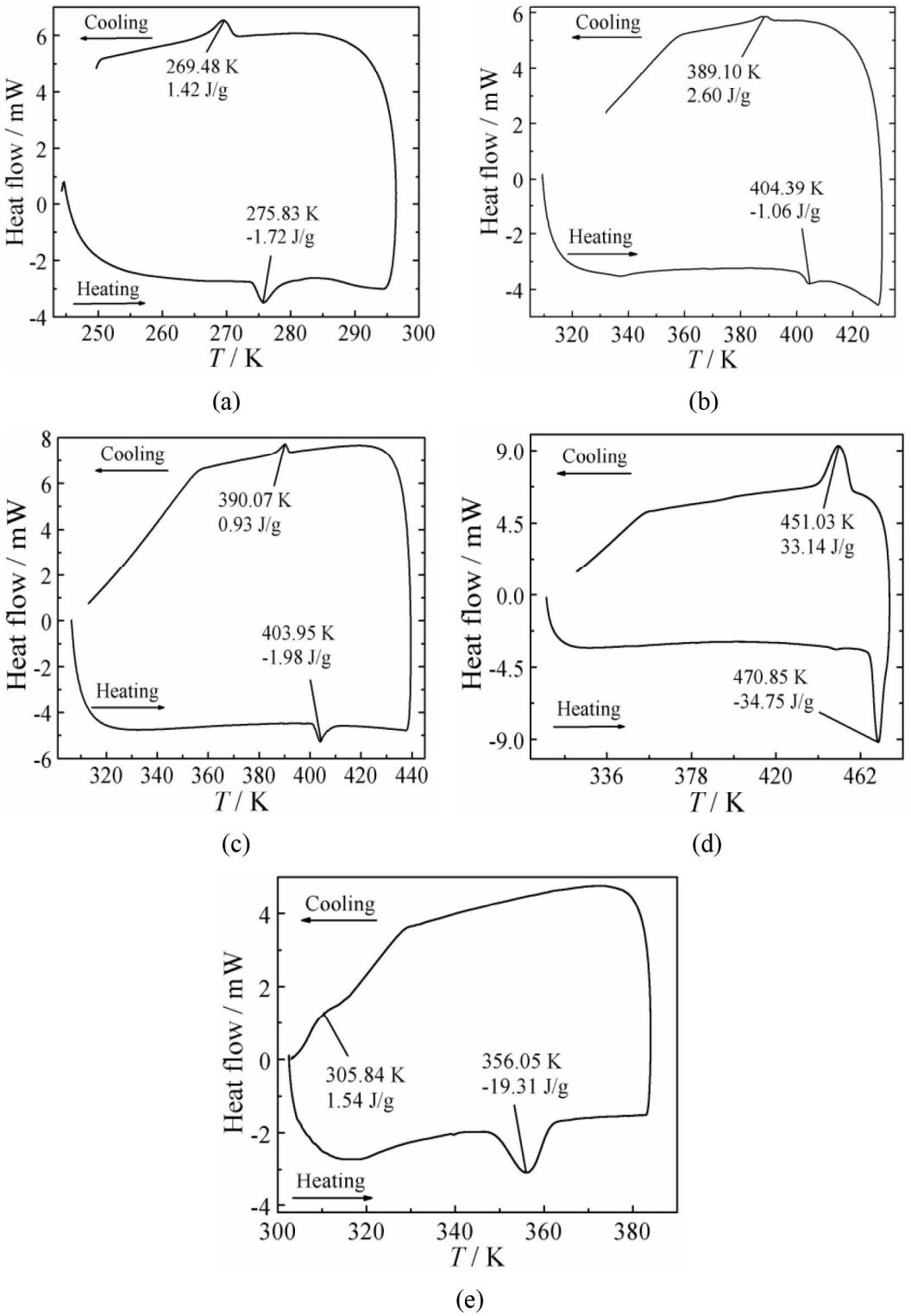

Figure 4.3 DSC measurement plots for compounds **3** (a); **4** (b); **7** (c); **9** (d) and **10** (e) showing the reversible transitions.

Phase transitions are also observed in compounds **3**, **6**, **7** and **10** using DSC measurements which are related to the thermochromic behavior (Figure 4.4). Interestingly many A_2CuCl_4 compounds are known for such structural transitions which leads to the thermochromic behavior. The two thermochromic transitions orange phase to (T = 294 K) yellow phase and to (T = 214 K) green phase are already reported in literature for compound **3** [15]. While no thermochromic records were found for compounds **6**, **7** and **10**. To observe thermochromic behavior in other OIHCs we heated the compounds near to their transition temperature in open air. As per our expectation we observed, yellow-green ↔ orange for compound **6**, yellow ↔ orange for compound **7** and green ↔ dark brown for compound **10**, as shown in Figure 4.4. This transition is reversible in nature and observed after repeated heating-cooling cycles. But we did not observed any measurable change for other OIHCs. This optical behavior is consistent with the transitions observed in the DSC measurements. The transitions for compound **10** can be of structural or solvation-desolvation nature and studied using EPR. Since, TG/DTA measurements have shown a small weight loss around this transition temperature, we thought the possibility for the solvation-desolvation nature. To confirm this possibility; we performed optical study under vacuum and under forced air. Interestingly, we observed reversible color changes every time. That means this transition is not related to adsorbed or coordinated solvent molecule, but might be related to structural transitions. We would like to mention here that recently thermochromic behavior is observed in yellow benzimidazolium tetrachlorocuprate (II), $(C_7H_7N_2)_2CuCl_4$ compound due to the absorption-desorption of water molecules where $CuCl_4^{2-}$ species existed in discrete tetrahedra [20]. Since $CuCl_4^{2-}$ species being stereochemically non-rigid, it can have any average Cl-Cu-Cl bond angle, ranging from 180º for square planar complexes to 109.58º for tetrahedral complexes. Its geometry as well as the color can typically be described by the average trans angle. It exhibits yellow-green color at RT when the trans angle is 140º. The color changes to dark green when this angle increases and orange as it decreases. Therefore, in present case (compound **10**), we believe that trans angle changes drastically below 140º [21]. To the best of our knowledge, changes from yellow to green (or vice versa) are well reported in literature but no data is available for green to dark brown.

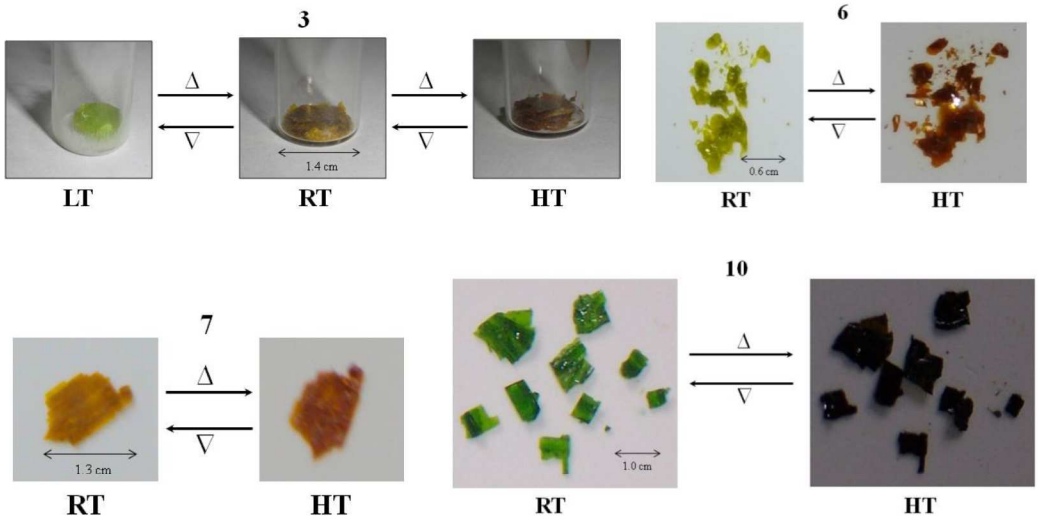

Figure 4.4 Thermochromic behavior of single crystals for compounds **3**, **6**, **7** and **10**.

4.3.5 Raman Spectra

Figure 4.5 illustrates temperature dependent Raman study for compound **3** which shows five Raman modes at 73 cm^{-1}, 96 cm^{-1}, 178 cm^{-1}, 257 cm^{-1} and 287 cm^{-1} in the low frequency region below 400 cm^{-1} at RT. These Raman modes are intense in lattice mode regions and bring out important information about dynamic of the transition. For instance, with lowering the temperature Raman modes at 73 cm^{-1} and 96 cm^{-1} changes in the background noise, Rayleigh scattering. These Raman modes at 73 cm^{-1} and 96 cm^{-1} increases together to give the new Raman modes at 88 cm^{-1} between the 260 K - 270 K. Compound **3** also shows the clear emergence of Raman mode centered around 130 cm^{-1} between 260 K - 270 K due to change in Rayleigh scattering. This means temperature dependent Raman spectroscopy also shows the solid-solid phase transition at temperature range 260 K - 270 K for compound **3**. This transition is reversible in nature and can be repeated for many cycles without any change.

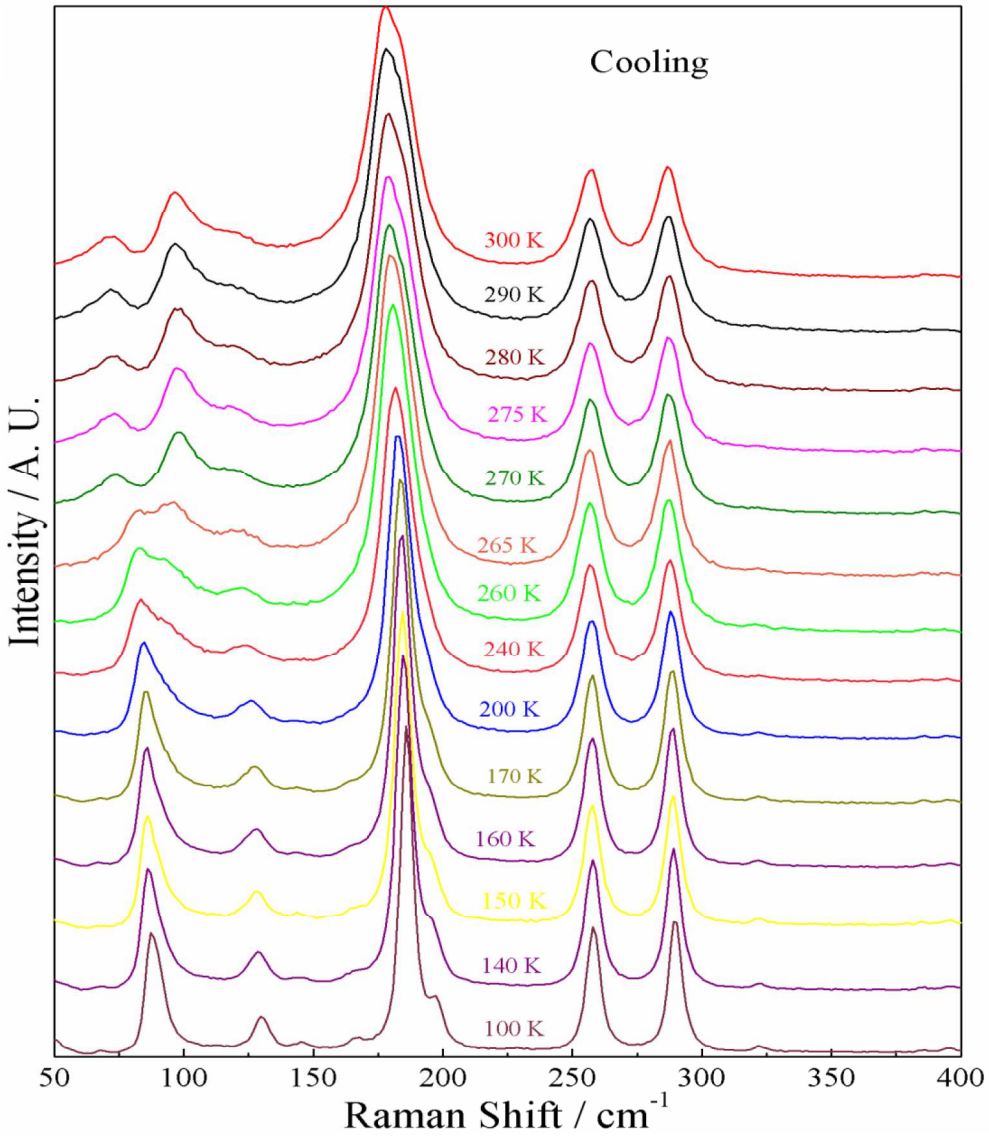

Figure 4.5 Temperature evolutions of lattice modes in compound **3**.

4.3.6 Electron Paramagnetic Resonance (EPR)

EPR spectra of copper complexes provide important information for studying the metal ion environment. At RT solid state EPR spectra consists of a single, no hyperfine structure. At RT *g*-values of $g_{\|}$ = 2.150 and $g_{\perp}$ = 2.071 were observed for copper (II) ion in compound **10**. The reported square planar complexes are having g values of $g_{\|}$ = 2.139 and $g_{\perp}$ = 2.053 at RT [22]. The *g*-values of compound **10** have also been estimated by L. Antolini *et al.*, who reported $g_{\|}$ = 2.130 and *g* = 2.050, these values are well agreed with our result [23]. The $g_{\|}$-factor variations evaluated from the powder EPR spectra are shown in Figure 4.6 (a).

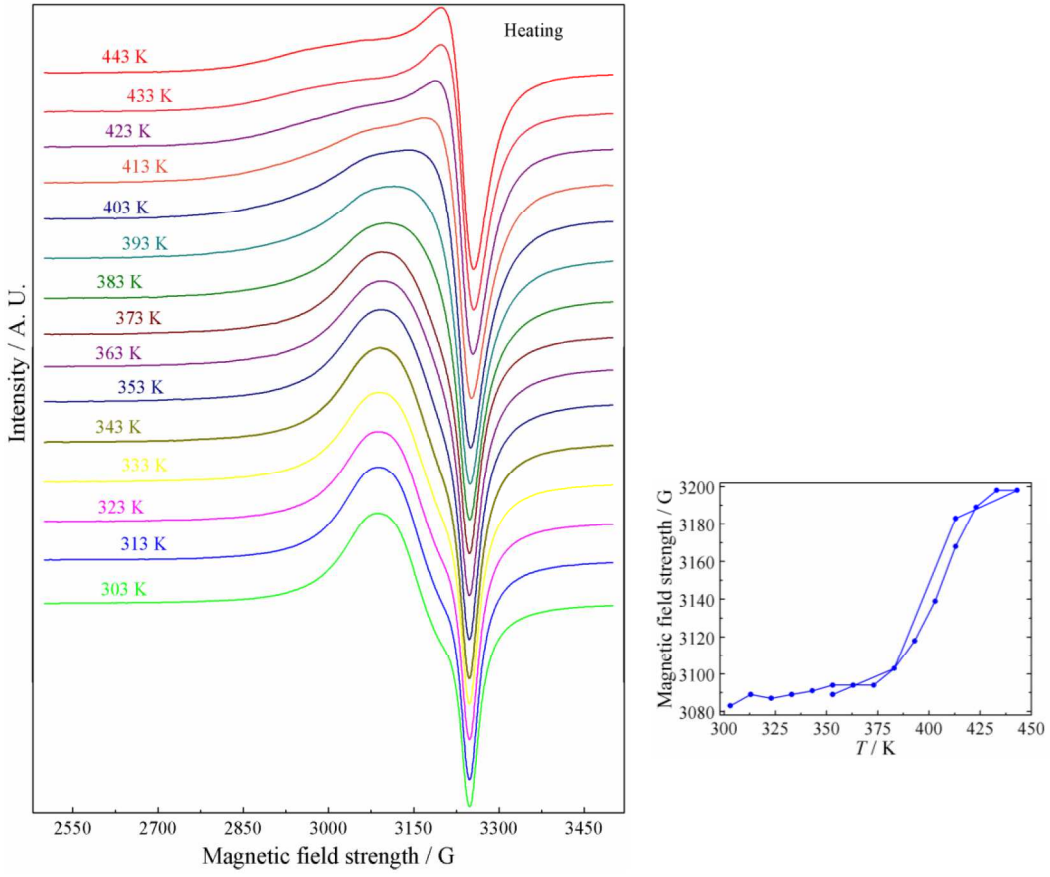

(a) (b)

Figure 4.6 Representative EPR spectra for compound **10** (a) and temperature dependent of EPR line widths (b), at HT.

The shift of the *g*-factors are from $g_{\|} = 2.150$ and $g\perp = 2.071$ (at RT) to $g_{\|} = 2.201$ and $g\perp = 2.182$ (at HT) respectively. The $g_{\|} = 2.201$ at HT agreed with flattened tetrahedral coordination of the copper atoms [24]. Temperature dependence of the EPR line widths are determined by the exchange of dipolar interaction. The large changes in width indicate a substantial decrease in the strength of the magnetic exchange coupling between the $CuCl_4^{2-}$ ions [Figure 4.6 (b)]. However, the nonlinear increase in width with temperature indicates that distortion to tetrahedral. The exact mechanism is unknown and it may be due to a thermally activated rigid body motion or distortion of the $CuCl_4^{2-}$ anions towards tetrahedral. The displacement of the 2-amino benzothiozilium cations weakened the hydrogen bonding (exchange coupling) or due to the combination of these effects. The changes in geometry of the $CuCl_4^{2-}$ chromophore account for thermochromic nature of the solid-solid phase transition.

4.3.7 Crystal Structure

4.3.7.1 Single Crystal X-ray Diffraction

Crystallographic data collection parameters and refinement data for compounds **2**, **3**, **8** and **10** are illustrated in Table 4.3 and 4.4. Figure 4.7 show the asymmetric unit consisting of compounds **2**, **3'**, **8** and **10'**.

Table 4.3 Crystallographic data and structure refinements for compounds **2** and **3**

Compounds	**2**	**3**	**3'**
Empirical formula	$C_{12}H_{14}Cl_4CuF_2N_2$	$C_{12}H_{14}Cl_6CuN_2$	$C_{12}H_{14}Cl_6CuN_2$
Formula weight	429.59	462.49	462.49
T (K)	150	298	150
Wavelength (Å)	0.71073	0.71073	0.71073
Crystal system	Monoclinic	Monoclinic	Orthorhombic
Space group	$P2_1/c$	$P2_1/c$	$Pccn$
a (Å)	15.5113(5)	16.4341(12)	7.3736(3)
b (Å)	7.3788(2)	7.3911(4)	32.0689(13)
c (Å)	7.0929(2)	7.2631(5)	7.1611(3)
β (°)	99.004(2)	101.576(4)	90
V (Å^3)	801.81(4)	864.28(10)	1693.34(12)
Z	2	2	4
D_{calc} (Mg/m^3)	1.779	1.177	1.814
Crystal size (mm^3)	0.27×0.17×0.08	0.37×0.23×0.09	0.37×0.23×0.09
F(000)	430	462	924
2θ range (°)	2.66 - 33.73	2.53 - 31.50	2.54 - 33.72
Index ranges	-21 ≤ h ≤ 24, -11 ≤ k ≤ 8, -11 ≤ l ≤ 11	-24 ≤ h ≤ 23, -10 ≤ k ≤ 10, -9 ≤ l ≤ 10	-11 ≤ h ≤ 11, -50 ≤ k ≤ 50, -10 ≤ l ≤ 11
Reflections collected	9039	7954	14172
Independent reflections	3169 [R_{int} = 0.0289]	2629 [R_{int} = 0.0285]	3373 [R_{int} = 0.0255]
Completeness to θ = 25.00°	99.2 %	99.3 %	99.6 %
Goodness-of-fit on F^2	1.025	1.011	1.124
Data / restraints / parameters	3169 / 0 / 125	2847 / 0 / 109	3373 / 0 / 125
Final R indices [I>2σ(I)]	$R1$ = 0.0329, w$R2$ = 0.0767	$R1$ = 0.0468, w$R2$ = 0.1297	$R1$ = 0.0257, w$R2$ = 0.0588
R indices (all data)	$R1$ = 0.0453, w$R2$ = 0.0821	$R1$ = 0.0535, w$R2$ = 0.1334	$R1$ = 0.0298, w$R2$ = 0.0601

Table 4.4 Crystallographic data and structure refinements for compounds **8** and **10**

Compounds	**8**	**10**	**10'**
Empirical formula	$C_{14}H_{18}Cl_6CuN_2$	$C_{14}H_{14}Cl_4CuN_4S_2$	$C_{14}H_{14}Cl_4CuN_4S_2$
Formula weight	490.54	507.75	507.75
T (K)	293	296	150
Wavelength (Å)	0.71073	0.71073	0.71073
Crystal system	Monoclinic	Monoclinic	Monoclinic
Space group	*Cc*	$P2_1/c$	$P2_1/c$
a (Å)	33.514(7)	7.0562(3)	6.9522(4)
b (Å)	5.2443(10)	9.7369(4)	9.6979(4)
c (Å)	10.572(2)	14.0321(6)	13.9366(6)
β (°)	98.933(3)	98.632(2)	97.849(3)
V (Å^3)	1835.7(6)	953.16(7)	930.83(8)
Z	4	2	2
D_{calc} (Mg/m^3)	1.775	1.796	1.812
Crystal size (mm^3)	0.42×0.17×0.10	0.32×0.18×0.11	0.32×0.18×0.11
F(000)	988	510	510
2θ range (°)	1.23 - 25.85	2.56 - 28.71	2.57 - 32.58
Index ranges	-40 ≤ h ≤ 40, -6 ≤ k ≤ 6, -12 ≤ l ≤ 12	-9 ≤ h ≤ 9, -13 ≤ k ≤ 13, -18 ≤ l ≤ 18	-10 ≤ h ≤ 7, -14 ≤ k ≤ 14, -20 ≤ l ≤ 21
Reflections collected	8782	9030	7985
Independent reflections	3526 [R_{int} = 0.0278]	2447 [R_{int} = 0.0215]	3355 [R_{int} = 0.0219]
Completeness to θ = 32.58°	99.9 %	99.6 %	98.9 %
Goodness-of-fit on F^2	1.236	1.042	1.071
Data / restraints / parameters	3526 / 2 / 208	2447 / 0 / 115	3355 / 0 / 115
Final R indices [I>2σ(I)]	*R1* = 0.0753, w*R2* = 0.2023	*R1* = 0.0283, w*R2* = 0.0704	*R1* = 0.0299, w*R2* = 0.0783
R indices (all data)	*R1* = 0.0792, w*R2* = 0.2059	*R1* = 0.0379, w*R2* = 0.0755	*R1* = 0.0383, w*R2* = 0.0818

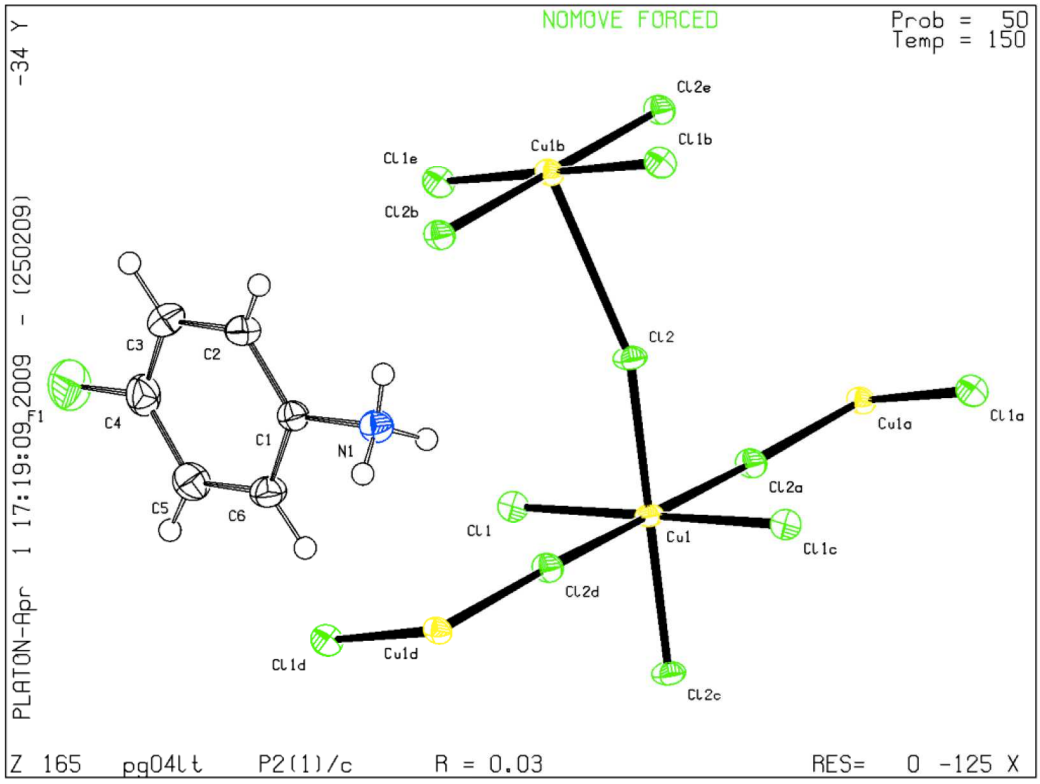
NOMOVE FORCED
Prob = 50
Temp = 150
PLATON-Apr 1 17:19:09 2009 - (250209) -34 Y
Z 165 pg04lt P2(1)/c R = 0.03 RES= 0 -125 X
Cl2e
Cl1b
Cu1b
Cl1e
Cl2b
Cl2
Cu1a
Cl1a
Cl2a
Cl1
Cu1
Cl1c
Cl2d
Cl1d
Cu1d
Cl2c
C3
C2
C4
C1
N1
C5
C6

(a)

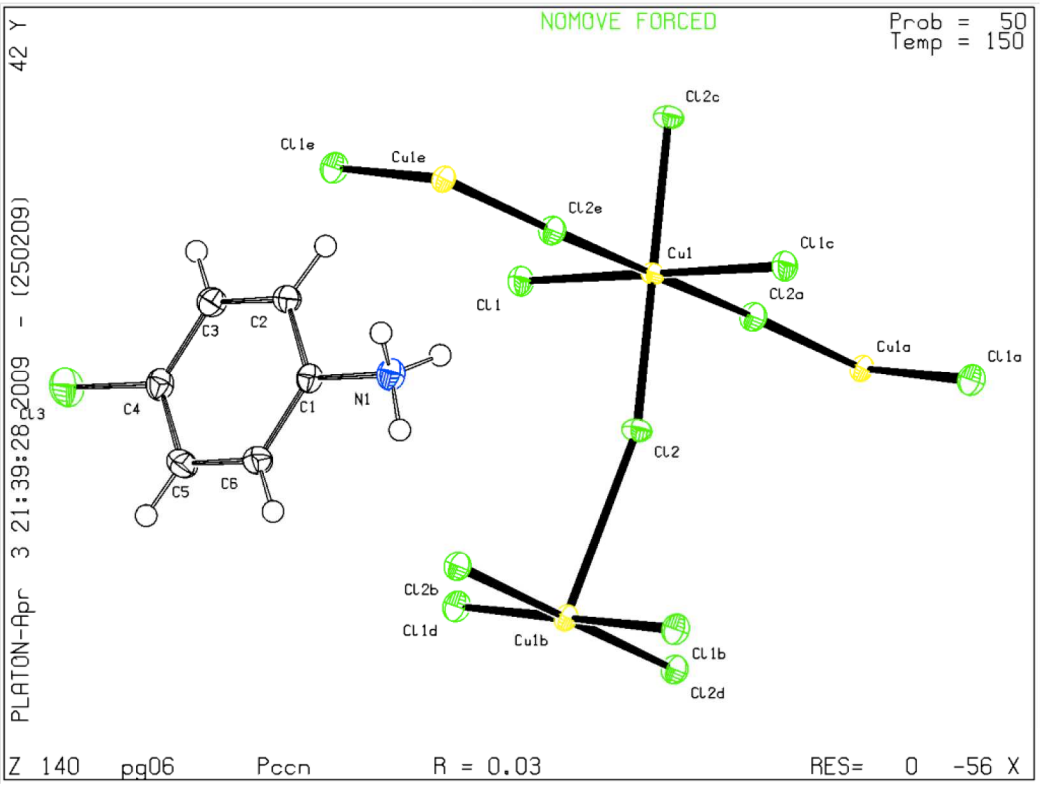
NOMOVE FORCED
Prob = 50
Temp = 150
PLATON-Apr 3 21:39:28 2009 - (250209) 42 Y
Z 140 pg06 Pccn R = 0.03 RES= 0 -56 X
Cl2c
Cl1e
Cu1e
Cl2e
Cu1
Cl1c
Cl1
Cl2a
Cu1a
Cl1a
Cl2
Cl2b
Cl1d
Cu1b
Cl1b
Cl2d
C3
C2
C4
C1
N1
C5
C6

(b)

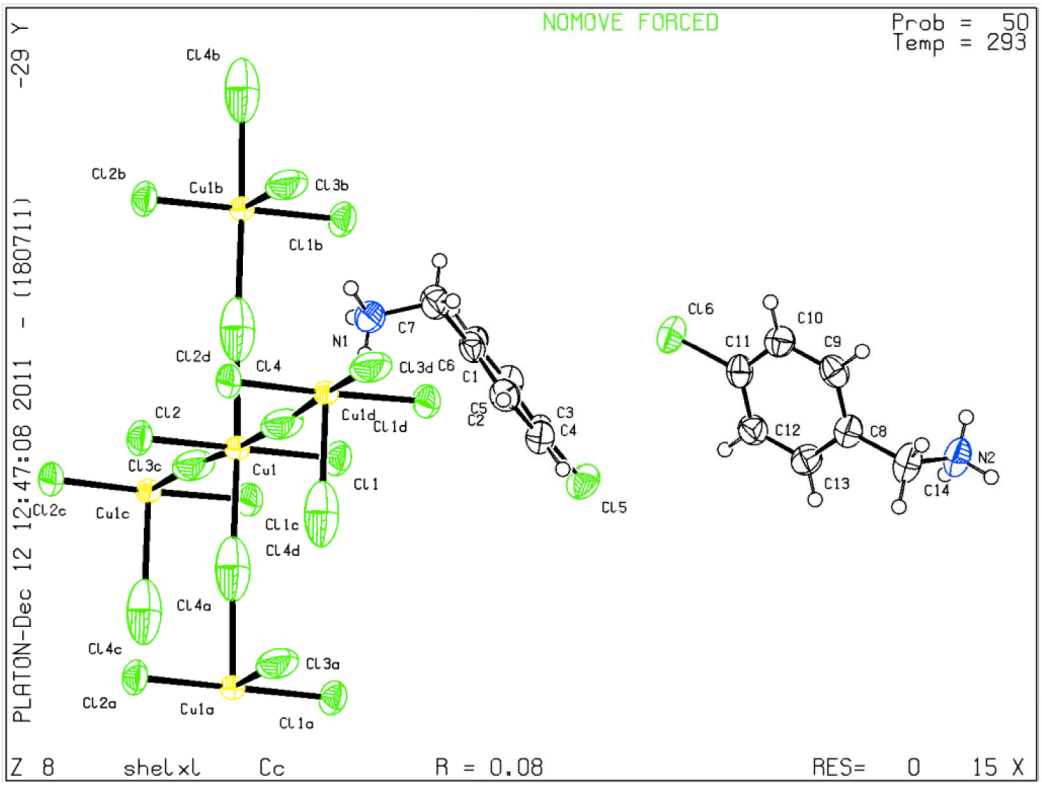

(c)

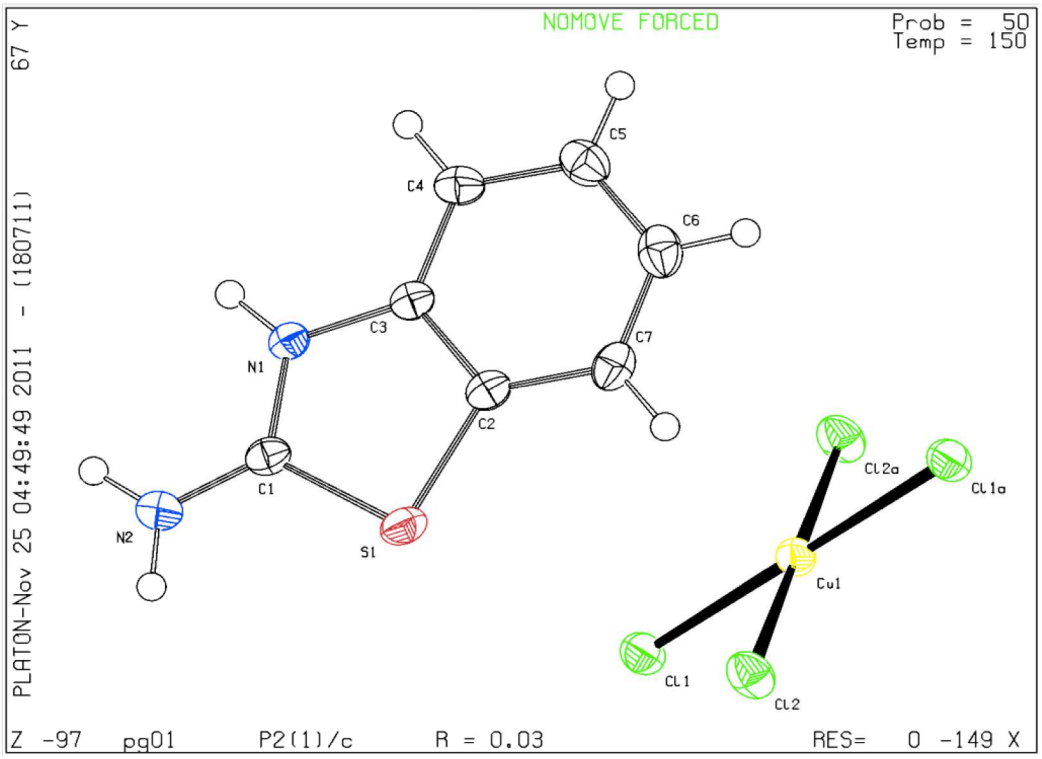

(d)

Figure 4.7 The structure of compounds **2** (a); **3'** (b); **8** (c) and **10'** (d) showing the asymmetric units.

Single crystal XRD analyses on OIHCs suggested that compounds **2**, **3** and **10** crystallizes in monoclinic space group $P2_1/c$ at 150 K and 298 K respectively. While **8** crystallize in monoclinic space group *Cc* at 293 K. The crystallographic data for these compounds are given in Table 4.3 and 4.4, and the structures of the asymmetric units for **2**, **3**, **8** and **10** are shown in Figure 4.7. The dianion of these OIHCs are planar and the Cl-Cu-Cl angles are close to 90º. The organic ammonium cations of these OIHCs are also nearly planar.

The structural analyses on these compounds show that **2**, **3** and **8** forms the layered structure of copper chloride. The structure of the copper-halide layer is characterized by two kinds of copper-halide distances equatorial (D_S) and axial (D_L) distances as a result of Jahn-Teller distortion see (Figure 4.8). In these layered perovskites Jahn-Teller elongated bonds on adjacent Cu^{2+} ions lie in the plane of the layer but are oriented at right angles to each other, defining an antiferrodistortive structure [25]. The values of D_S, D_L and interlayer distance are listed in Table 4.1. These values suggest small distortions from perfect octahedral geometries for the copper ions. As expected, the interlayer distance between inorganic layers for compound **2** is smaller than that for compounds **3**, **3'** and **8** due to smaller radius of fluoride ion as compared to chloride ions and size of the organic ammonium cations. The interlayer distance between inorganic layers for compounds **3** and **3'** are also smaller than that for compound **8** due to the size of the organic ammonium cations.

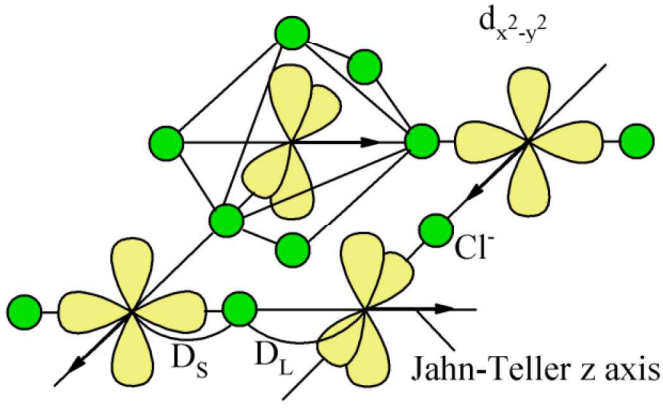

Figure 4.8 The layered structure of $CuCl_4$.

Surprisingly, single crystal XRD data collected on compound **3** at 150 K (**3'**), shows structural phase transition from the monoclinic space group $P2_1/c$ to the

orthorhombic space group *Pccn*. The lattice parameters of compounds **3** and **3'** are listed in Table 4.3. The DSC analyses also show the presence and reversibility of this transition with a transition temperature at around 276 K. Though, the basic structure remains constant for both compounds with $(CuCl_4^{2-})_n$ layers sandwiched between anilinium ions moieties. A closer look at the crystal structures on these compounds revealed a few characteristic differences. Figure 4.9 represent the packing in the structures of compounds **2**, **3**, **3'** and **8** along with the crystallographic *a*-axis and *b*-axis. In the case of compounds **3** and **3'** the adjacent layers A and B are related by an inversion center and in addition there is a 2-fold screw axis parallel to the *b*-axis and *a*-axis respectively. Consequently, the molecular axis of the cations in the neighbouring layers A and B appear parallel in compound **3**. While in the case of compound **2** there is a small distortion and in compound **8** there is a large distortion because of that there is an absent of inversion center between A and B layers and they are related by a 2-fold screw axis operation parallel to the *c*-axis. Therefore, A and B layers are slightly tilted in compounds **2** and **8** similar to the observed for (4-chloro anilinium)$_2$CuBr$_4$ [17].

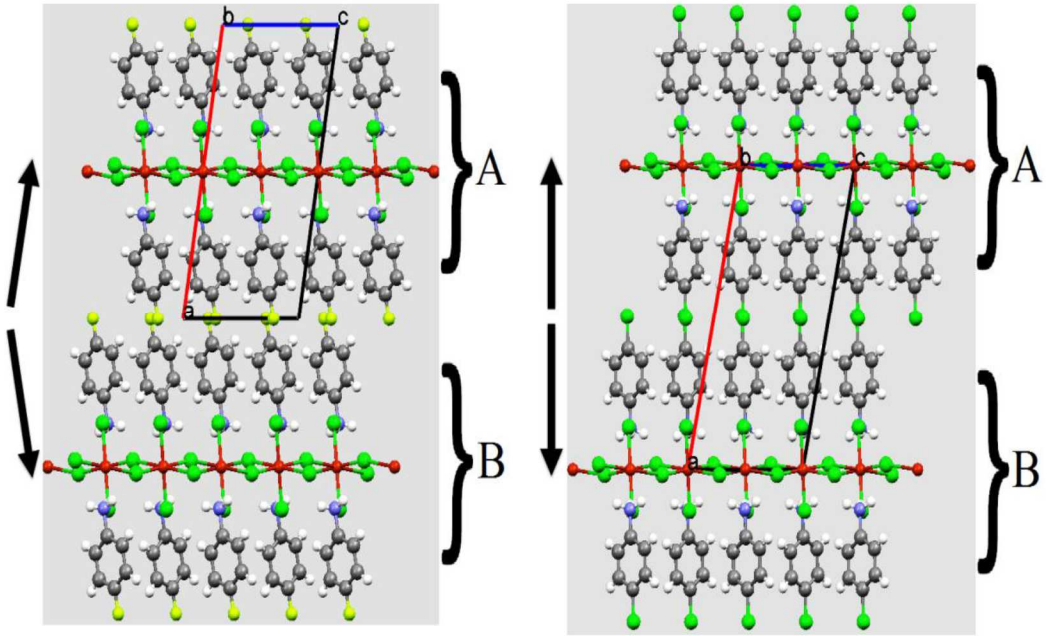

(a) (b)

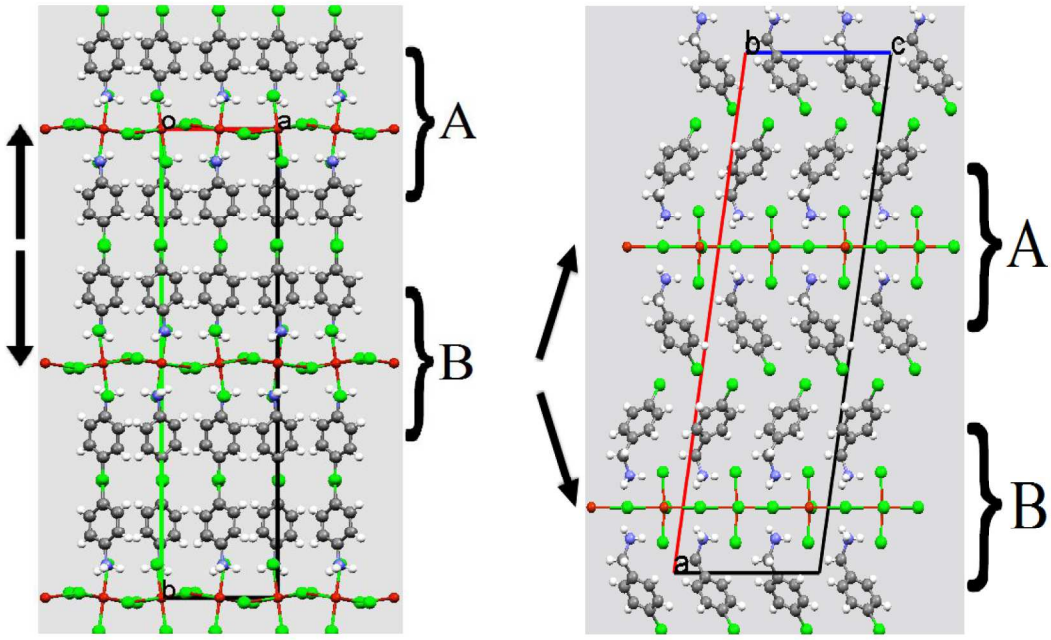

(c) (d)

Figure 4.9 The layered structures for compounds **2** (a); **3** (b); **3'** (c) and **8** (d), viewed along the crystallographic *b*-axis and *c*-axis.

According to literature [25], monoammonium organic cation compounds prefer the staggered configuration by displacing each successive perovskite sheets, while diammonium cation compounds should adopt an eclipsed configuration. In the later case the organic cations make hydrogen bond to the inorganic sheets at both ends and thereby removing the van der Waals gap between the layers. Therefore in the real structures the manner in which organic cations make hydrogen bond to the inorganic sheets influences the alignment of adjacent layers. In the present case as shown in Figure 4.10, the 2-D inorganic layers of '$CuCl_4$' anions adopt an eclipsed and staggered conformation. Figure 4.11 and Table 4.5 represent three hydrogen bonding interactions (N-H···Cl) for compound **2**, three hydrogen bonding interactions for compound **3** and one hydrogen bonding interaction for compound **8** between the ammonium head and Cl from the inorganic layer. In the case of compound **2**, three hydrogen bonding interactions, two with terminal Cl atoms and one with a bridging Cl atom are found. Compound **3** shows only two such hydrogen bonding interactions, one with a terminal Cl and the other with a bridging Cl atom. On the other hand compound **8** shows one hydrogen bonding interaction with one bridging Cl atom.

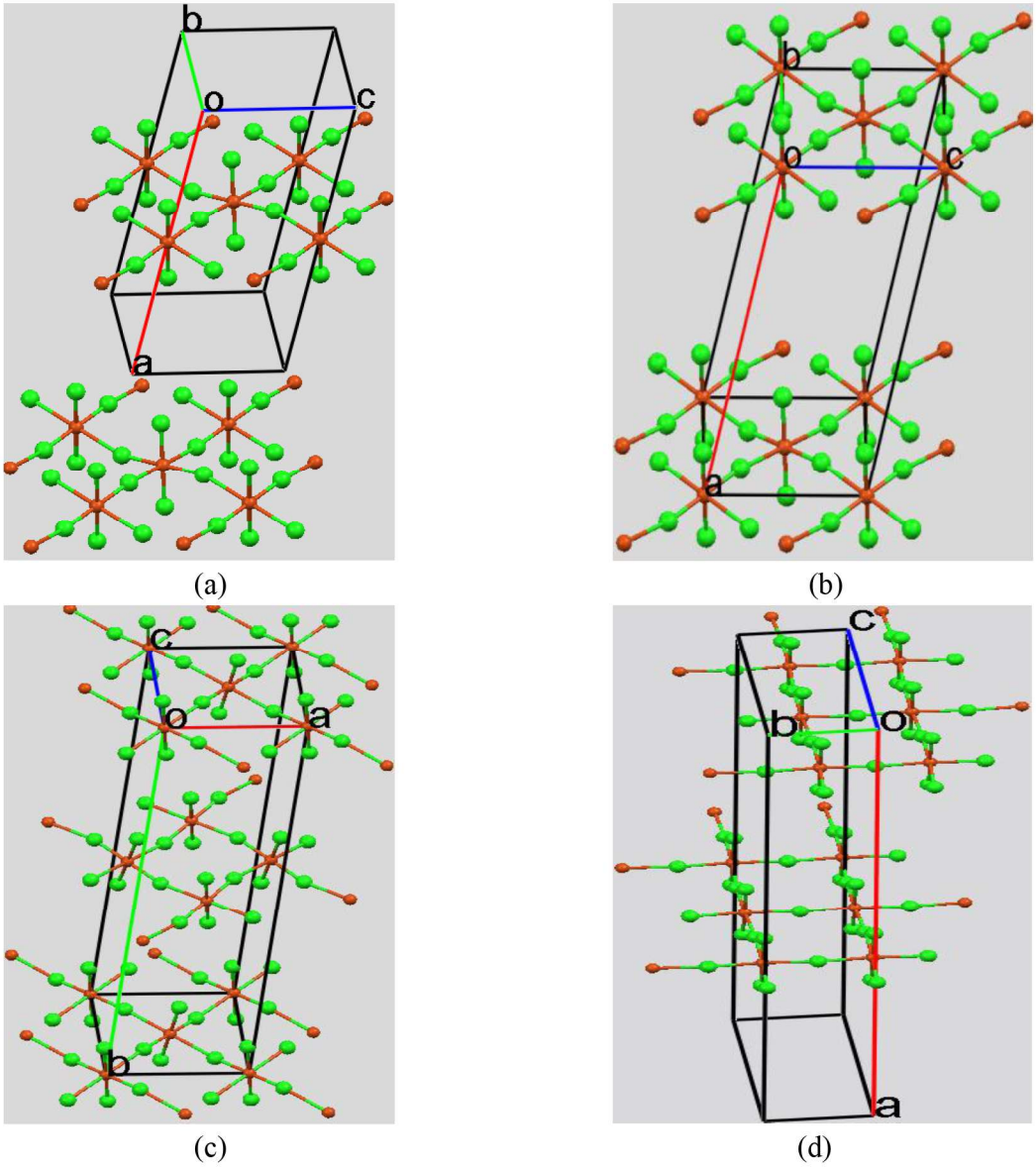

Figure 4.10 The "eclipsed" and "staggered" conformations of the inorganic 2-D network for compounds **2** (a); **3** (b); **3'** (c) and **8** (d).

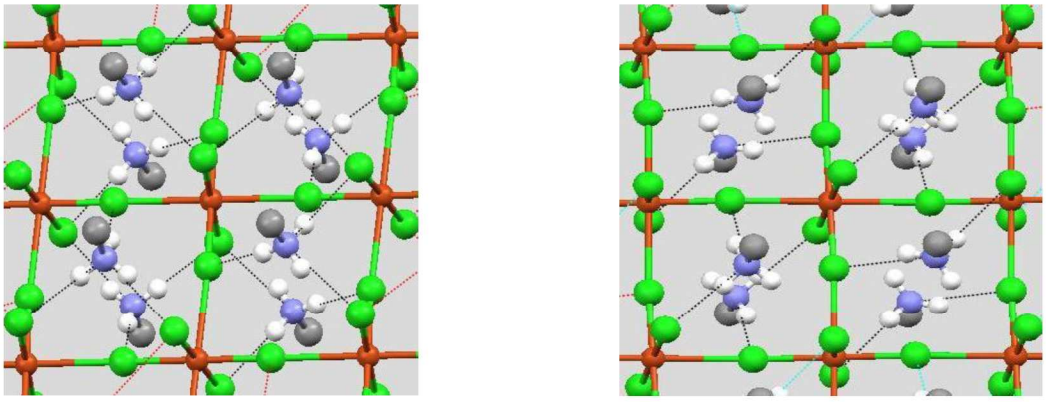

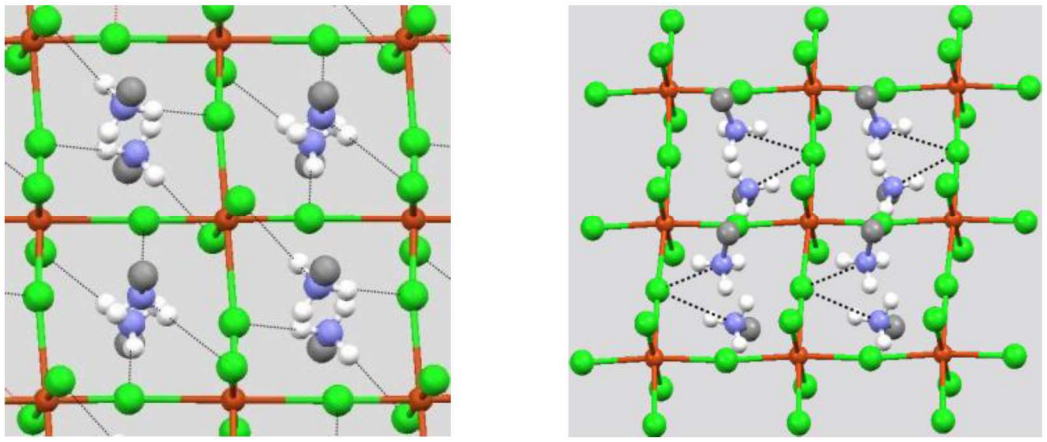

(c) (d)

Figure 4.11 N-H···Cl hydrogen bonding interactions for compounds **2** (a); **3** (b); **3'** (c) and **8** (d).

Furthermore, single crystal XRD data were measured at 296 K and 150 K for compound **10** [23]. The single crystal structures in this compound consisted of layered distorted perovskite type structures where $CuCl_4^{2-}$ remained separate having square-planar geometry. Single crystal XRD analysis reveals that an asymmetric unit consists of a half of the $(CuCl_4)^{2-}$ dianion together with a 2-aminobenzothiazolium cation. The Cu atom of the dianion is located on a twofold symmetry axis, the chlorine atoms and all atoms of the 2-aminobenzothiazolium cation are situated on general positions. Therefore, there are two 2-aminobenzothiazolium cations for each of the dianion giving the stoichiometry $2(C_7H_7N_2S):CuCl_4$. The protonated hydrogen atom is clearly apparent on the thiazole nitrogen atom and the C=N double bond is reasonably well ordered as the associated bond distances. The C-N single bond involving a benzo carbon (C3) atom is 1.392(2) Å and the C=N bond is 1.333(2) Å. The two ions are held together by weak hydrogen bonding interactions (see Table 4.5) involving the chlorides and one of the amino hydrogen atom and ring thiazolium hydrogen atom. Literature has sited many isolated $CuCl_4^{2-}$ compounds. Most of them have tetrahedral or distorted square planar structures, which concluded that the present compound is one of the 'rare' square planar $CuCl_4^{2-}$ complex [26].

Table 4.5 Hydrogen bonds and angles for OIHCs [Å and °]

Compounds	Distance [N···Cl]	Distance [H···Cl]	Angle [NH···Cl]
2	3.241(2)	2.395(3)	166.85(3)
	3.266(1)	2.458(4)	159.94(3)
	3.187(1)	2.339(3)	158.64(2)
3	3.292(3)	2.431(9)	161.91(7)
	3.282(3)	2.400(8)	156.97(7)
3'	3.245(1)	2.359(2)	167.61(2)
	3.217(1)	2.372(2)	157.41(2)
8	3.296(5)	2.558(3)	140.70(3)
	3.295(5)	2.549(3)	141.80(3)
10	3.260(2)	2.509(2)	146.5(1)
	3.205(2)	2.353(2)	171.0(1)
	3.143(2)	2.305(2)	164.5(1)
10'	3.195(2)	2.323(2)	171.2(1)
	3.237(2)	2.465(2)	146.8(1)
	3.128(1)	2.270(1)	164.9(1)

CCDC No. 756479, 756480, 882749 and 793784 contains the crystallographic data for the compounds **2**, **3'**, **8** and **10'**. This data can be obtained free of charge via http://www.ccdc.cam.ac.uk/conts/retrieving.html, or from the Cambridge Crystallographic Data Centre, 12 Union Road, Cambridge CB2 1EZ, UK; fax: (+44) 1223 336 033; or e-mail: deposit@ccdc.cam.ac.uk.

4.3.7.2 Powder X-ray Diffraction

Powder XRD pattern of compounds **4**, **5**, **6** and **7** at RT are shown in Figure 4.12. The powder pattern of compound **4** was indexed using powder X5 software. These powder patterns were indexed in triclinic, lattice type *P* with unit cell a = 8.864(2) Å, b = 13.721(3) Å, c = 15.925(3) Å, α = 89.690(3) Å, β = 96.020(5) Å, γ = 102.110(4) Å, V = 1879.87(3) Å^3, R factor = 0.001 for compound **4** with 2θ error 0.08. The powder XRD analysis of compound **4** represents that it crystallizes in triclinic system which is slightly different from those reported in the previous study [11]. Moreover, the powder XRD pattern for compounds **5**, **6** and **7** at RT shows that the powder XRD patterns were almost similar with previous study as shown in Figure 4.13.

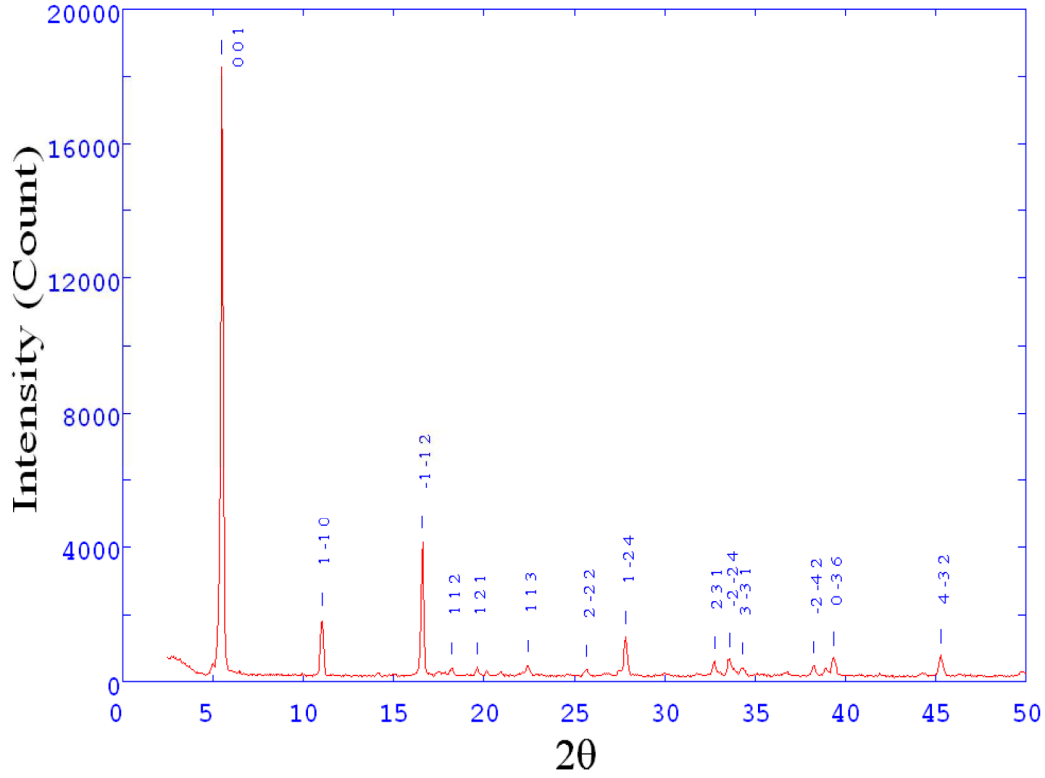

Figure 4.12 Powder XRD data for compound **4**.

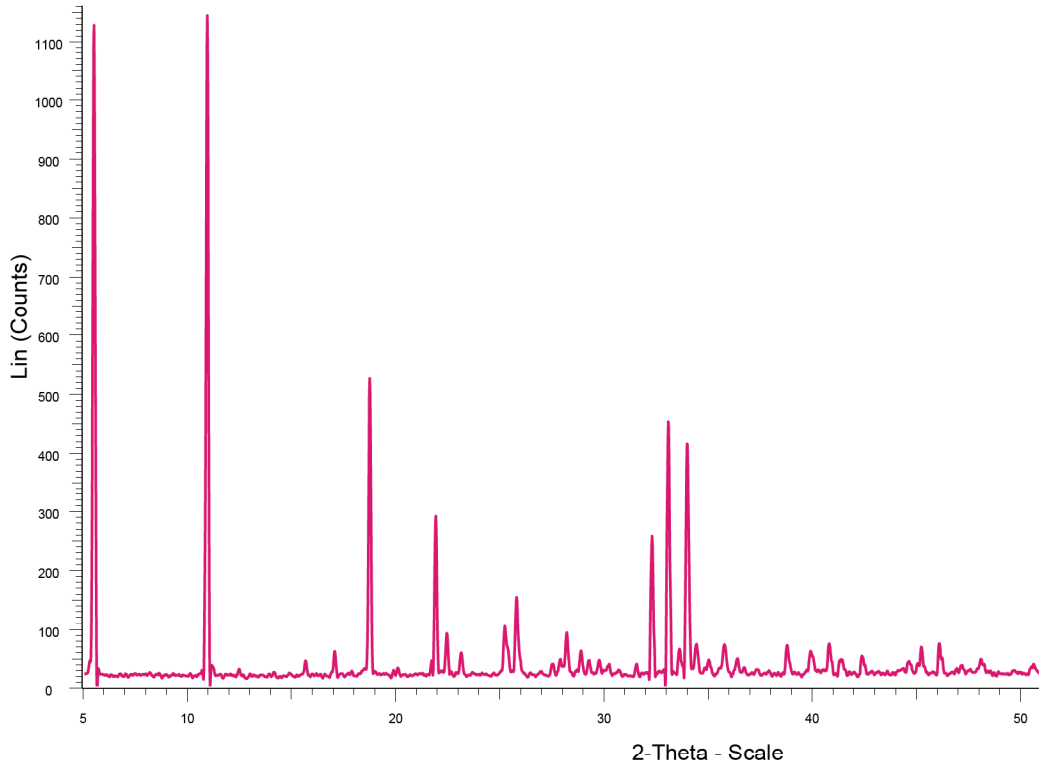

(a)

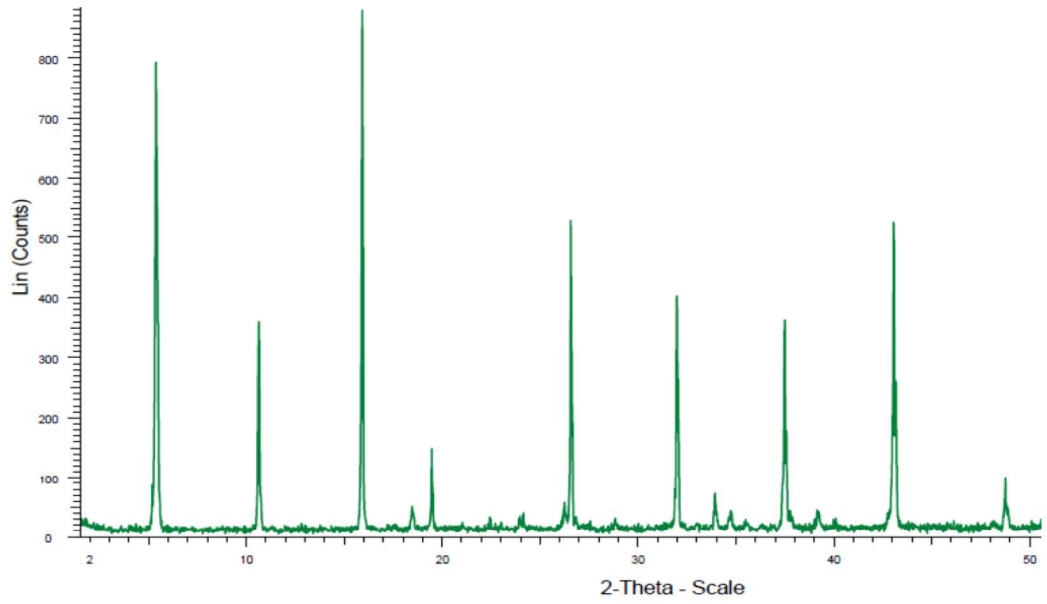

(b)

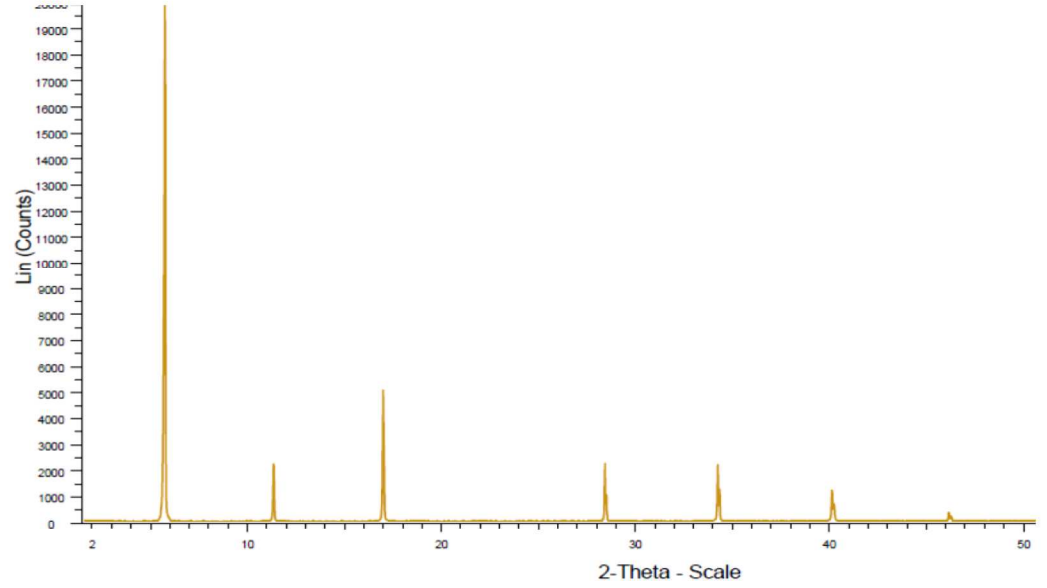

(c)

Figure 4.13 Powder XRD data for compounds **5** (a); **6** (b) and **7** (c).

4.3.8 Magnetic Properties

Figure 4.14 illustrates the temperature dependence of the product of the magnetic susceptibility with temperature (χT) measured under different magnetic fields for few OIHCs. The observed χT value for compounds **2, 3, 4, 5, 6** and **10** are 0.453 cm^3 K mol^{-1}, 0.431 cm^3 K mol^{-1}, 0.421 cm^3 K mol^{-1}, 0.433 cm^3 K mol^{-1}, 0.414 cm^3 K mol^{-1} and 0.395 cm^3 K mol^{-1} obtained at 300 K, in good agreement with the expected value for one Cu^{2+} ion with $S = ½$ and $g = 2.0023$ (0.375 cm^3 K mol^{-1}).

A gradual increase of the χT product upon cooling is observed from 300 K to 20 K. Below this temperature there is a sharp increase of the χT product for compounds **2**, **3**, **4**, **5** and **6**. A rounded maximum is obtained at around 9 K for compound **2** and **3**, 6 K for compound **4** and 8 K for compound **5** and **6**, which decline on further cooling. These features are typical of ferromagnetic interaction and/or spin canting behavior [27]. Since all Cu^{2+} ions in this network are crystallographically generated in a centrosymmetric space group, we could not correlate the behavior with the spin canting phenomenon. The turnover in the value of χT at LT is probably due to weak antiferromagnetic couplings between layers and saturation magnetization. The temperature dependence susceptibility plot also reflects the spontaneous magnetization present as a consequence of long range ordering of Cu^{2+} ions within the layers below the 16 K for these OIHCs shown as an inset in Figure 4.14. Figure 4.15 shows a plot of χ^{-1} versus T (K) for these OIHCs, which obey the Curie-Weiss law above 30 K with positive θ values of 73 K, 51 K, 26 K, 17 K and 28 K for compounds **2, 3, 4, 5** and **6** respectively.

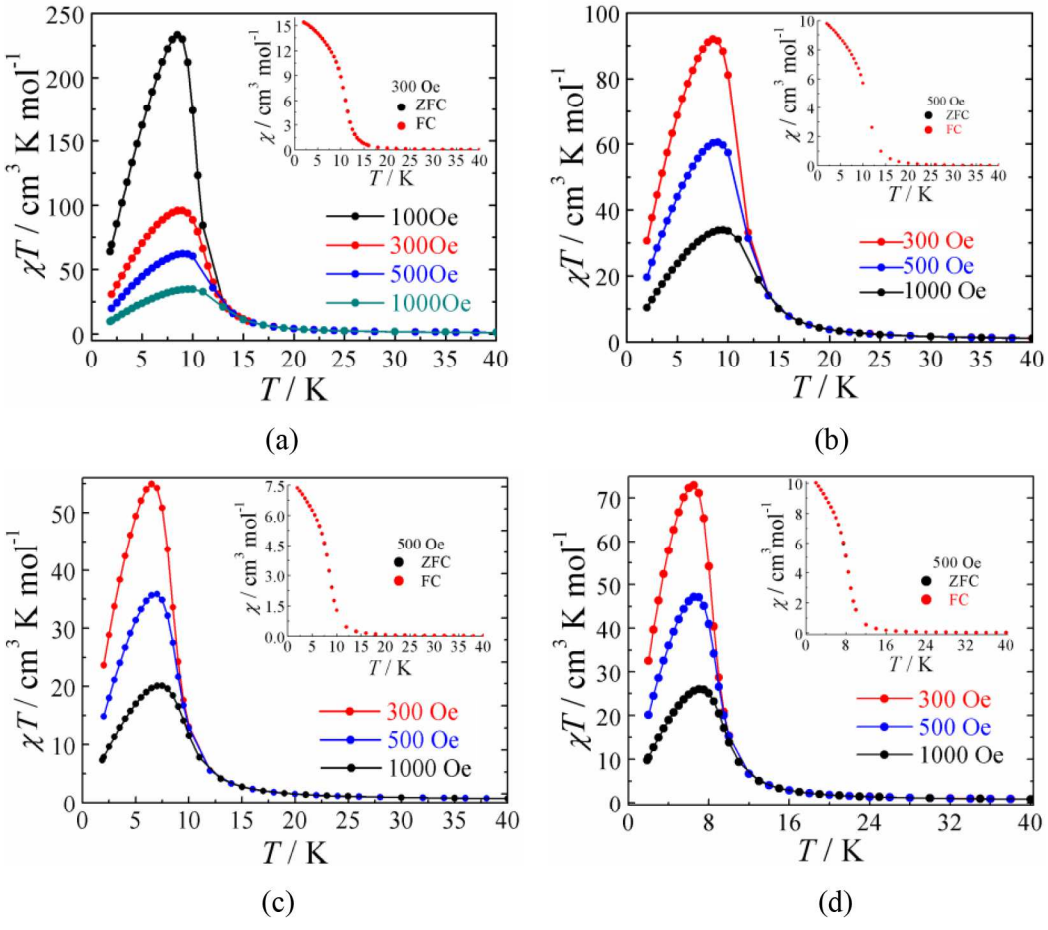

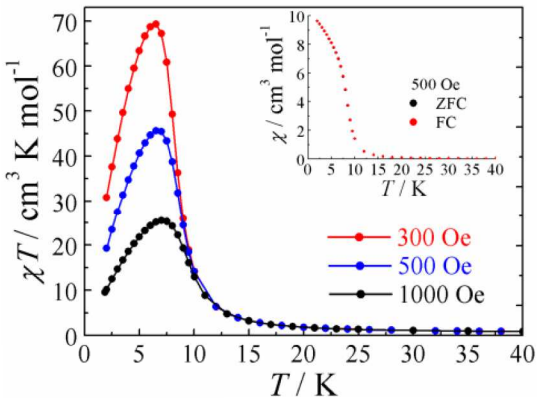

(e)

Figure 4.14 Temperature dependence χT with different applied fields for compounds **2** (a); **3** (b); **4** (c); **5** (d) and **6** (e).

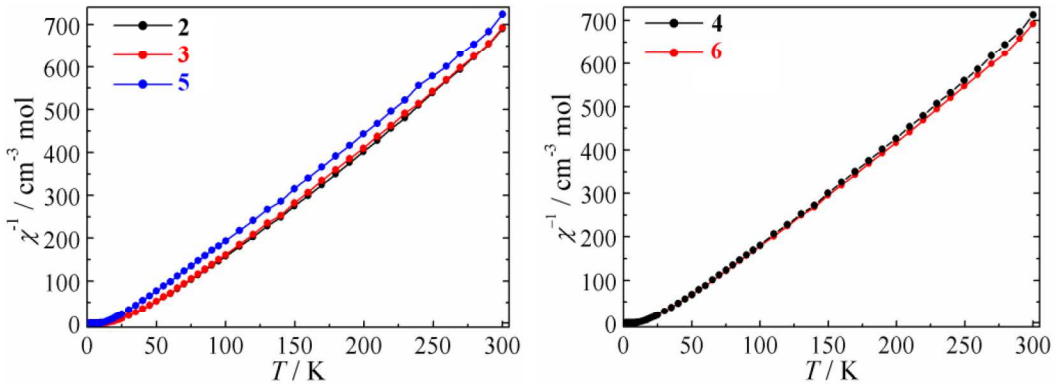

(a) (b)

Figure 4.15 The temperature dependence χ^{-1} plot for compounds **2**, **3**, **5** (a) and **4**, **6** (b) obeying the Curie-Weiss law above the 30 K.

Figure 4.16 represent the field dependence of the magnetization for OIHCs. It reveals the sharp increase at low fields and tends to saturate below 15 kOe. The saturation of magnetization reached approx 1.04 μ_B, 1.05 μ_B, 0.143 μ_B, 0.785 μ_B and 1.008 μ_B for compounds **2**, **3**, **4**, **5** and **6** respectively, less than expected 1.73 for Cu^{2+} ion. The slightly lower than expected spin-only saturation value is due to the interlayer antiferromagnetic interaction. The very small saturations value 0.143 μ_B for compound **4** indicates the presence of dominant antiferromagnetic interaction. The hysteresis effects observed in all layered OIHCs are characteristic of soft ferromagnet. Inset in Figure 4.16 shows the hysteresis loop in the low-field region, for clearly showing soft magnetic behavior.

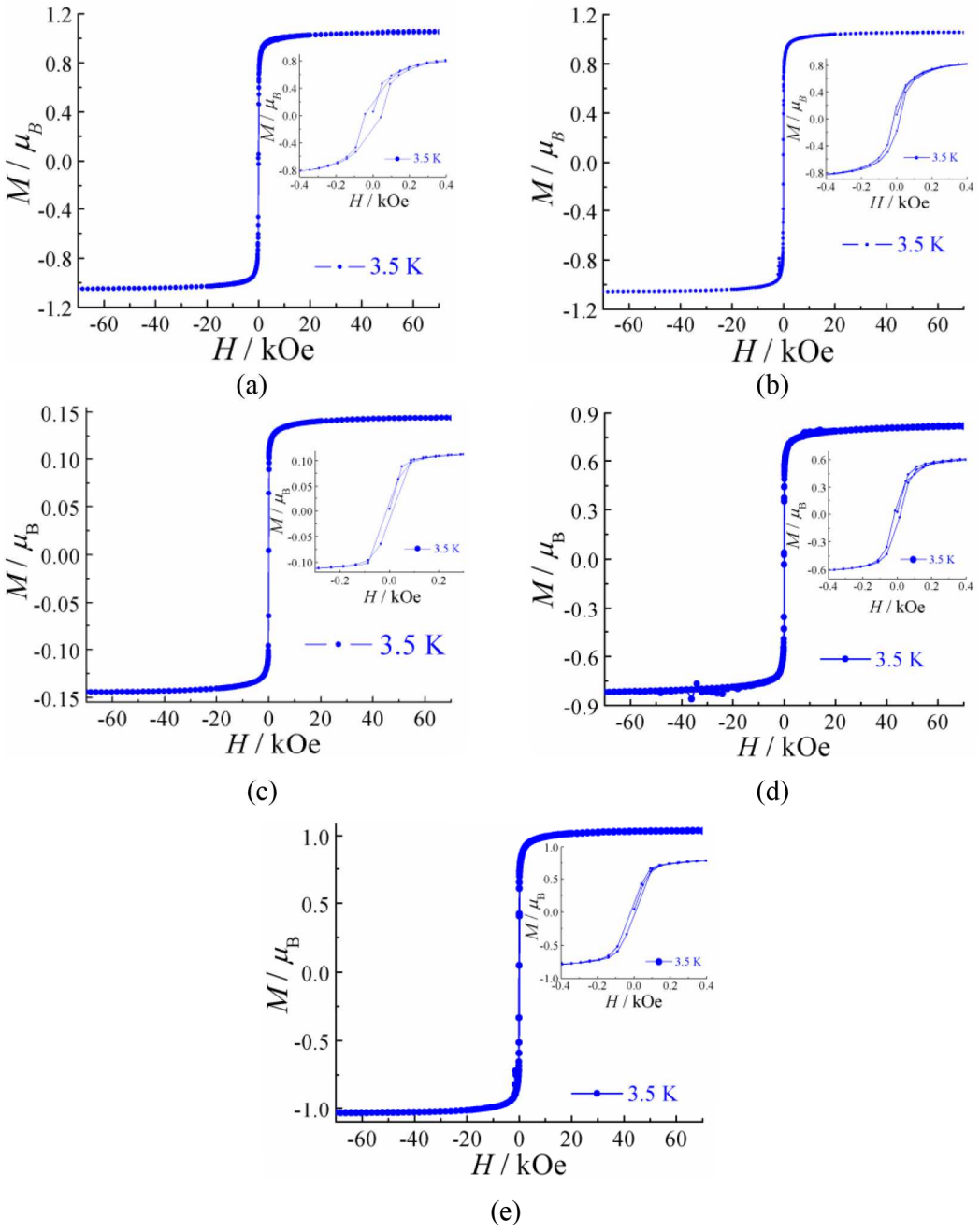

Figure 4.16 The *M-H* plots for compounds **2** (a); **3** (b); **4** (c); **5** (d) and **6** (e) measured at 3.5 K. The inset shows the hysteresis loop in the low field region.

Ac-susceptibility measurements for all OIHCs were performed to confirm this ferromagnetic ordering and to determine precisely the critical temperature (T_C). Figure 4.17 illustrates the magnetic susceptibility real (in-phase) and imaginary (out-of-phase) components as a function of temperature for selected frequencies of 10 Hz, 100 Hz, 200 Hz, 500 Hz, 800 Hz and 1200 Hz at 0 Oe. The in-phase ac-magnetic

susceptibility (χ') exhibits a rounded maximum at 11 K for compounds **2**, **3** and 9 K for compounds **4**, **5**, **6**. The out-of-phase ac susceptibility (χ'') shows onset of a long range magnetic ordering at 9.0 K for compounds **2**, **3** and 7 K for compounds **4**, **5**, **6** respectively. The weak frequency dependent behavior suggests that the long range magnetic ordering appears below a critical temperature in all OIHCs. Although the structural changes observed in compound **3** with a variation of temperature does not lead to any observable changes in the magnetic behavior.

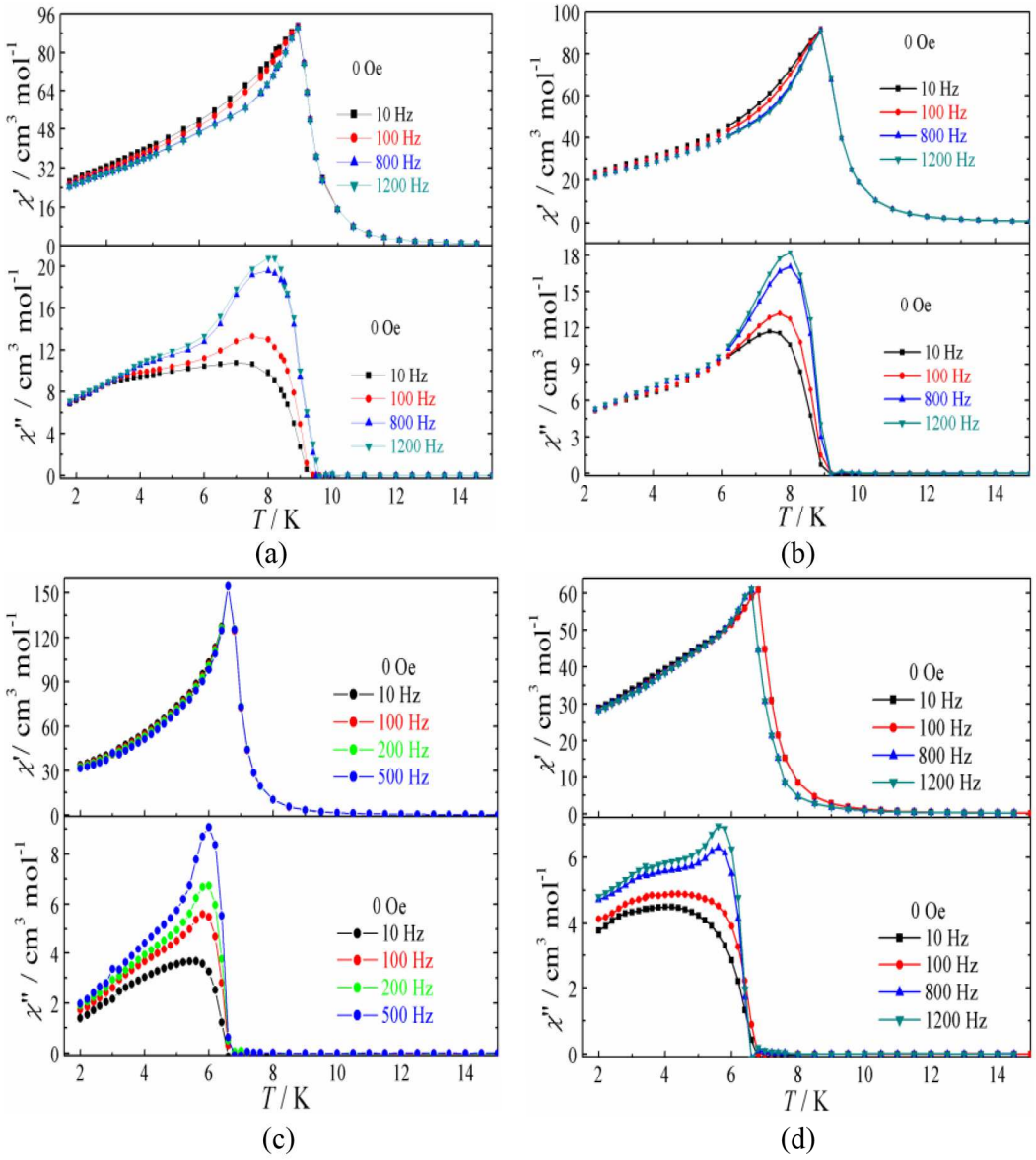

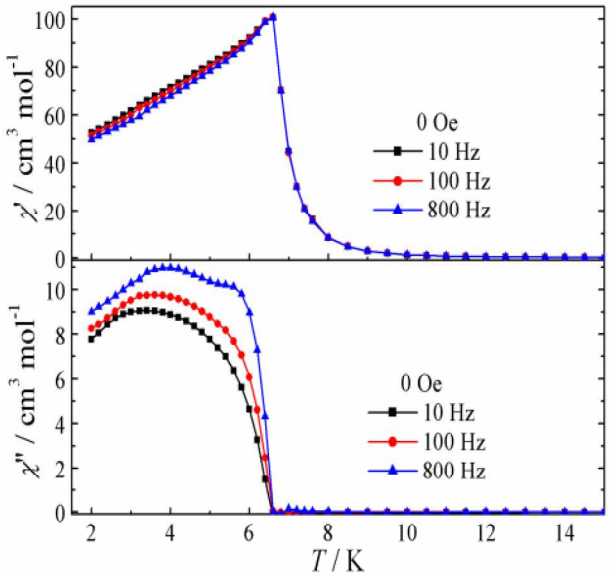

(e)

Figure 4.17 Temperature dependence of the ac-susceptibility for compounds **2** (a); **3** (b); **4** (c); **5** (d) and **6** (e).

It is also expected that square planar coordination geometry of the Cu (II) complex, that is a d^9 species, should be paramagnetic. This is confirmed by the shape of temperature-dependent magnetic susceptibility measurements (at field of 1000 Oe, 500 Oe and 300 Oe), using SQUID magnetometer, typical of a paramagnetic material, compound **10** as shown in Figure 4.18 (a). The plot of χT versus T, shows χT value at 300 K to be 0.395 cm^3 K mol^{-1} [slightly greater than expected 0.375 cm^3 K $mole^{-1}$ for Cu^{2+} ions]. χT shows a marginal increase upon cooling ca. 15 K and subsequent decrease for lower temperatures as shown in inset of Figure 4.18 (a). At RT the effective magnetic moment, μ_{eff}, was found to be 1.77 μ_B, very close to the value of 1.73 μ_B predicted for independent $S = ½$ spins with $g_{Cu} = 2.0023$ see Figure 4.18 (b). The magnetic interactions is very weak due to the anionic counterparts are isolated by the diamagnetic benzothiazole cations, as shown in the crystal structure. This is in good agreement with the magnetization isothermal obtained at 1.8 K, see Figure 4.18 (a) inset. At high applied magnetic fields the magnetization saturates at a value of 1.0149 $N\mu_B$, in good agreement with the calculated value of $M_S = gS = 1.015\ N\mu_B$.

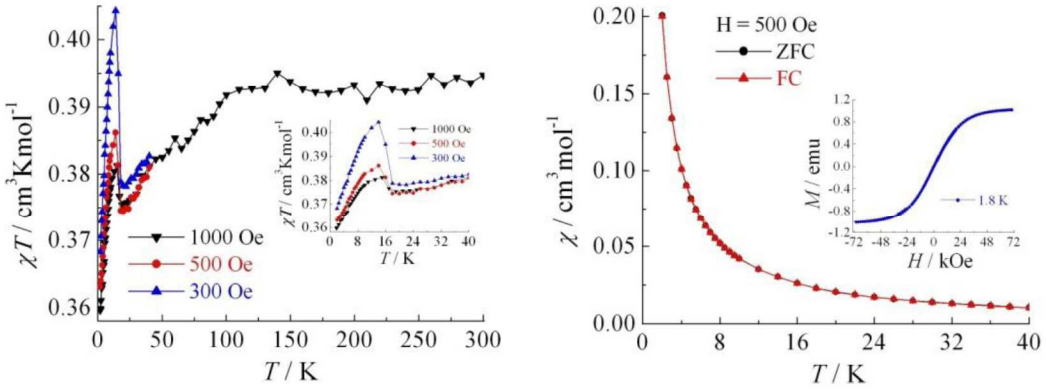

(a) (b)

Figure 4.18 Variations of χT as function of temperature, inset with enlarge scale in the LT (a) and variation of χ as function of temperature using 500 Oe, inset shows M versus H at 1.8 K (b).

4.4 Conclusion

- Synthesized and characterized ten OIHCs using FT-IR, CHN analysis, single XRD or powder XRD analysis.
- OIHCs were investigated for reversible solid-solid structural phase transition using thermal studies (DSC), temperature dependent Raman and EPR measurements, and single crystal XRD.
- TG/DTA measurements showed different degradation paths in OIHCs, where compounds **1**, **3**, **5**, **6** and **8** loses organic ammonium chloride along with amine, while compounds **2**, **4** and **9** showed first loss for organic ammonium chloride. On the other hand compound **7** have shown first loss of hydrochloride instead of benzilinium chloride and compound **10** shows the bulk loss for 2-aminobenzothiozole.
- DSC measurements on OIHCs showed endothermic peaks at 275.83 K, 404.39 K, 410.50 K, 403.95 K, 470.85 K and 356.05 K for compounds **3**, **4**, **6**, **7**, **9** and **10**, respectively with thermochromic change, characteristic for solid-solid structural phase transition.
- Temperature dependent Raman spectroscopy for compound **3** shows the solid-solid structure phase transition in the temperature range 260 K - 270 K.

- EPR spectrum for compound **10** shows with increasing temperature, dynamic disorder of cations weakens the hydrogen bonding, causing Cl-Cl electrostatic repulsions to distort the $CuCl_4^{2-}$ ions further toward a tetrahedral geometry.
- Most of the OIHCs crystallized in the layered structure, where $CuCl_4^{2-}$ forms a layer and OACs are flanked on both sides to complete octahedra around Cu^{2+}.
- Compound **3** shows structural transition from monoclinic space group $P2_1/c$ at 296 K, isostructurally to, compounds **1**, **2** and **10**, orthorhombic space group *Pccn* at 150 K and resembles very much with compounds **7**, **8**. Single crystal XRD for compound **3** showed "eclipsed" conformations at 296 K and "staggered" conformations at 150 K for the 2-D network of inorganic layer $CuCl_4^{2-}$.
- The dc and ac-magnetic susceptibility measurements using a SQUID magnetometer suggested that these are soft ferromagnet, with interlayer antiferromagnetic behavior.
- Compound **10**, which is square planar and has isolated structure showed paramagnetic behavior.

References

[1] G. D. Sprol, G. D. Stucky, *Inorg. Chem.* **1972**, *11*, 1647-1650.

[2] R. D. Willett, F. Waldner, *J. Appl. Phys.* **1982**, *53*, 2680-2682.

[3] **A. K. Vishwakarma**, P. S. Ghalsasi, A. Navamoney, Y. Lan, A. K. Powell, *Polyhedron* **2011**, *30*, 1565-1570.

[4] B. Dolling, A. L. Gillon, A. G. Orpen, J. Starbuck, X. -M. Wang, *J. Chem. Soc. Chem. Commun.* **2001**, *6*, 567-568.

[5] J. Ishikawa, T. Asaji, D. Nakamura, *J. Magn. Reson.* **1983**, *51*, 95-102.

[6] K. Horiuchi, *Phys. Status. Solidi* **2004**, *A201*, 723-726.

[7] **A. K. Vishwakarma**, P. S. Ghalsasi, *J. Therm. Ana. Calorim.* **2012**, *107*, 155-158.

[8] A. Purkayashtha, J. B. Baruah, *Thermochim. Acta* **2002**, *390*, 187-193.

[9] M. G. El-Shaarawy, *J. Magn. Magn. Mater.* **2000**, *217*, 93-98.

[10] R. Belka, *J. Mater. Sci.* **2007**, *42*, 10090-10097.

[11] D. A. Tucker, P. S. White, K. L. Trojan, M. L. Kirk, W. E. Hatfield, *Inorg. Chem.* **1991**, *30*, 823-826.

[12] M. M. Zhao, P. P. Shi, *Acta Cryst. E* **2010**, *66*, m656.

[13] K. P. Larsen, *Acta Chem. Scand. A* **1974**, *28*, 194-200.

[14] R. D. Willett, *J. Chem. Phys.* **1964**, *41*, 2243-2244.

[15] M. F. Mostafa, M. M. Abdel-Kader, S. S. Arafat, E. M. Kandeel, *Physica Scripta*. **1991**, *43*, 627-629.

[16] A. Z. Mohamed, S. S. Saleem, M. A. El-Ghandour, M. A. Ahmed, *J. Mater. Sci.* **1993**, *28*, 1289-1292.

[17] T. Sekine, T. Okuno, K. Awaga, *Inorg. Chem.* **1998**, *37*, 2129-2133.

[18] A. O. Polyakov, A. H. Arkenbout, J. Baas, G. R. Blake, A. Meetsma, A. Caretta, P. H. M. van Loosdrecht, T. T. M. Palstra, *Chem. Mater.* **2012**, *24*, 133-139.

[19] M. Textor, E. Dubler, H. R. Oswald, *Inorg. Chem.* **1974**, *13*, 1361-1365.

[20] R. Bhattacharya, M. S. Ray, R. Dey, L. Righi, G. Bocelli, A. Ghosh, *Polyhedron* **2002**, *21*, 2561-2565.

[21] P. Zanchini, R. D. Willett, *Inorg. Chem.* **1990**, *29*, 3027-3030.

[22] M. V. Angeluşiu, G. L. Almăjan, D. C. Ilieş, T. Roşu, M. Negoiu, *Chem. Bull. Politehnica* **2008**, *53*, 1-2.

[23] L. Antolini, A. Benedetti, A. C. Fabretti, A. Giusti, *Inorg. Chem.* **1988**, *27*, 2192-2194.

[24] D. W. Smith, *Coord. Chem. Rev.* **1976**, *21*, 93-158.

[25] D. B. Mitzi, *J. Chem. Soc., Dalton Trans.* **2001**, 1-12.

[26] S. R. Desjardins, K. W. Penfield, S. L. Cohen, R. L. Musselman, E. I. Solomon, *J. Am. Chem. Soc.* **1983**, *105*, 4590-4603.

[27] D. J. Price, F. Lionti, R. Ballou, P. T. Wood, A. K. Powell, *Phil. Trans. R. Soc. Lond. A* **1999**, *357*, 3099-3118.